Quaternary Science Reviews 32 (2012) 48–63

Contents lists available at SciVerse ScienceDirect

Quaternary Science Reviews

journal homepage: www.elsevier.com/locate/quascirev

Paleomagnetism of Quaternary sediments from Lomonosov Ridge and Yermak Plateau: implications for age models in the Arctic Ocean

Chuang Xuan [a,*], James E.T. Channell [a], Leonid Polyak [b], Dennis A. Darby [c]

[a] Department of Geological Sciences, University of Florida, 241 Williamson Hall, P.O. Box 112120, Gainesville, FL 32611, USA
[b] Byrd Polar Research Center, Ohio State University, Columbus, OH 43210, USA
[c] Department of Ocean, Earth, and Atmospheric Sciences, Old Dominion University, Norfolk, VA 23529, USA

ARTICLE INFO

Article history:
Received 2 February 2011
Received in revised form
15 November 2011
Accepted 17 November 2011
Available online 10 December 2011

Keywords:
Lomonosov Ridge
Yermak Plateau
Magnetic excursions
Titanomaghemite
Self-reversal

ABSTRACT

Inclination patterns of natural remanent magnetization (NRM) in Quaternary sediment cores from the Arctic Ocean have been widely used for stratigraphic correlation and the construction of age models, however, shallow and negative NRM inclinations in sediments deposited during the Brunhes Chron in the Arctic Ocean appear to have a partly diagenetic origin. Rock magnetic and mineralogical studies demonstrate the presence of titanomagnetite and titanomaghemite. Thermal demagnetization of the NRM indicates that shallow and negative inclination components are largely "unblocked" below ~300 °C, consistent with a titanomaghemite remanence carrier. Following earlier studies on the Mendeleev–Alpha Ridge, shallow and negative NRM inclination intervals in cores from the Lomonosov Ridge and Yermak Plateau are attributed to partial self-reversed chemical remanent magnetization (CRM) carried by titanomaghemite formed during seafloor oxidation of host (detrital) titanomagnetite grains. Distortion of paleomagnetic records due to seafloor maghemitization appears to be especially important in the perennially ice covered western (Mendeleev–Alpha Ridge) and central Arctic Ocean (Lomonosov Ridge) and, to a lesser extent, near the ice edge (Yermak Plateau). On the Yermak Plateau, magnetic grain size parameters mimic the global benthic oxygen isotope record back to at least marine isotope stage 6, implying that magnetic grain size is sensitive to glacial–interglacial changes in bottom-current velocity and/or detrital provenance.

1. Introduction

Sediment cores from the Arctic Ocean commonly record intervals of shallow to negative magnetic inclination, typically tens of centimeters thick. These negative and intervening positive inclination intervals were initially interpreted as polarity chronozones implying very low (fractions of mm to few mm per kyr) deposition rates throughout the central Arctic Ocean (e.g., Steuerwald et al., 1968; Clark, 1970; Hunkins et al., 1971; Herman, 1974; Witte and Kent, 1988). When alternative age models emerged, it became clear that sedimentation rates were probably an order of magnitude higher (Løvlie et al., 1986; Darby et al., 1997; Jakobsson et al., 2000, 2001, 2003; Backman et al., 2004; Spielhagen et al., 2004; Kaufman et al., 2008; Polyak et al., 2009). Accordingly, the negative inclination intervals were attributed to geomagnetic excursions within the Brunhes Chron (e.g., Løvlie et al., 1986; Jakobsson et al., 2000; Spielhagen et al., 2004; O'Regan et al., 2008).

A number of geomagnetic excursions within the last few million years have been reported worldwide from deep-sea or lake sediment cores, lavas, and loess. At least seven magnetic excursions are reasonably well documented in the Brunhes Chron (Champion et al., 1988; Langereis et al., 1997; Worm, 1997; Lund et al., 2001, 2006; Laj and Channell, 2007). The higher fidelity magnetic excursion records with high quality age constraints generally yield excursion durations of <5 kyr (see Laj and Channell, 2007). For instance, the duration of the Laschamp excursion, the best known excursion in the Brunhes Chron, was estimated to be ~1.5 kyr by Laj et al. (2000) using a chronology based on correlation of a marine $\delta^{18}O$ record to the GISP2 (Greenland) ice core. A few-kyr duration for excursions is consistent with the model of Gubbins (1999) who proposed that "during excursions the field may reverse in the liquid outer core, which has timescales of 500 years or less, but not in the solid inner core, where the field must change by diffusion with a timescale of 3 kyr". In the unlikely case that the outer core reversed field survives for >3 kyr, diffusion into the inner core gives rise to the long-lived polarity chron or subchron. Due to the brief duration of geomagnetic excursions (nominally <3 kyr), and smoothing effects of the sediment magnetization lock-in process,

* Corresponding author. Now at: College of Oceanic and Atmospheric Sciences, Oregon State University, 104 COAS Admin Building, Corvallis, OR 97331, USA.
E-mail address: cxuan@coas.oregonstate.edu (C. Xuan).

0277-3791/$ – see front matter © 2011 Elsevier Ltd. All rights reserved.
doi:10.1016/j.quascirev.2011.11.015

sediments would need to maintain deposition rates of at least 5–10 cm/kyr to record geomagnetic excursions (e.g., Roberts and Winklhofer, 2004).

Sediments deposited in the Brunhes Chron from the Arctic Ocean and the Norwegian–Greenland Sea have appeared to be anomalously efficient in recording geomagnetic excursions for sediments with mean deposition rates of a few cm/kyr. Nowaczyk et al. (2001) recognized six excursions in three cores from the Makarov Basin in the central Arctic Ocean, close to the Lomonosov Ridge (Cores PS 2178 and PS 2180; Fig. 1). For IODP (Integrated Ocean Drilling Program) Arctic Coring Expedition (ACEX) cores from the Lomonosov Ridge (Fig. 1), O'Regan et al. (2008) placed the Brunhes/Matuyama boundary at 10.82 m revised composite depth (rmcd) in accord with ^{10}Be stratigraphy and orbital tuning of bulk density and ARM/IRM data (ratio of anhysteretic remanent magnetization to isothermal remanent magnetization), implying a mean sedimentation rate of ~1.4 cm/kyr during the Brunhes Chron. Three apparent excursions in the upper 4.65 rmcd were associated with the Mono Lake/Laschamp excursion, the Norwegian–Greenland Sea excursion, and the Biwa II excursion, and eleven additional excursions were observed within the 4.65–10.82 rmcd interval (O'Regan et al., 2008). Near Yermak Plateau (Fig. 1), 3–4 intervals of negative inclination were observed in Cores PS 1533 and PS 2212 (Nowaczyk et al., 1994), and in Core PS 2138 (Nowaczyk and Knies, 2000), with age control provided by ^{14}C, δ^{18}O, ^{10}Be and ^{230}Th stratigraphies, and nannofossil biostratigraphy. The marine isotope stage (MIS) 5/6 boundary in these cores was often placed at a depth of ~4–5 m (Nowaczyk et al., 1994; Nowaczyk and Knies, 2000), indicating mean sedimentation rates of ~3 to 5 cm/kyr for the last ~130 kyr. Cores PS 1707, 1878, 1882, and 1892 from the Greenland Basin, north of Jan Mayen Island (Fig. 1), yielded negative remanence inclinations associated with the Mono Lake excursion, the Laschamp excursion, and the Biwa I excursion (Nowaczyk and Antonow, 1997), with mean sedimentation rates of ~2 to 4.5 cm/kyr estimated from planktic δ^{18}O-derived ages.

Cores from the Arctic Ocean and the Norwegian–Greenland Sea generally yield larger duration estimates for supposed geomagnetic

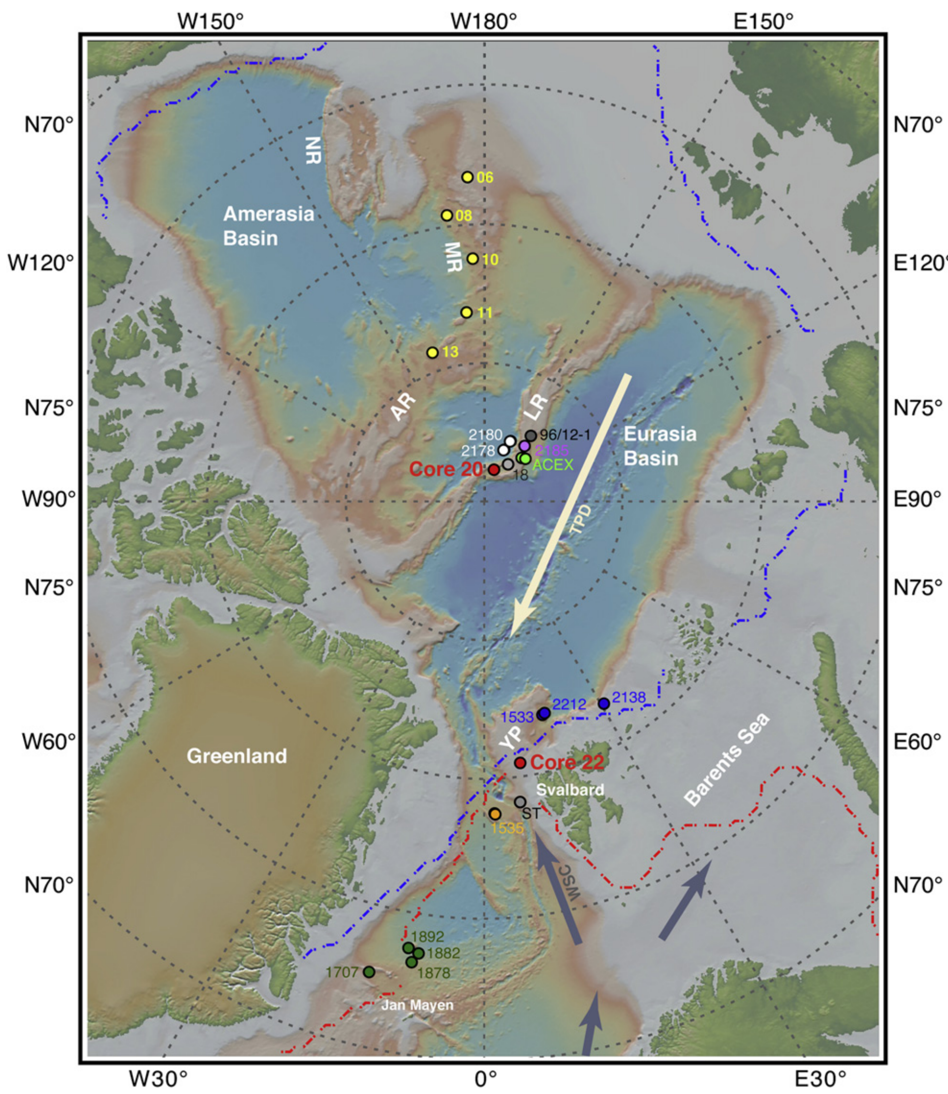

Fig. 1. Location of Cores 20 and 22 (red solid circles) retrieved by the HOTRAX'05 expedition, in comparison with location of previously studied cores. Base map data are from international bathymetric chart of Arctic Ocean (IBCAO, Jakobsson et al., 2008). Map is processed using the GeoMapApp© software. Labeled features are: Lomonosov Ridge (LR), Mendeleev Ridge (MR), Alpha Ridge (AR), Northwind Ridge (NR), Yermak Plateau (YP), Transpolar Drift (TPD, yellow arrow), and North Atlantic water inflows (gray arrows) including the West Spitsbergen Current (WSC). Blue and red dash dot lines are extent of sea ice of March and September medians for 1979–2000 (data from National Snow and Ice Data Center), respectively. References for previously studied cores listed on the map are as following. 06: Channell and Xuan, 2009; 08, 10, 11, and 13: Xuan and Channell, 2010; 18: Sellén et al., 2010; 2178 and 2180: Nowaczyk et al., 2001; 96/12-1: Jakobsson et al., 2000, 2001, 2003; 2185: Spielhagen et al., 2004; ACEX: Backman et al., 2008; O'Regan et al., 2008; 1533 and 2212: Nowaczyk et al., 1994; 2138: Nowaczyk and Knies, 2000; Nowaczyk et al., 2003; 1535: Nowaczyk et al., 2003; 1707, 1878, 1882, and 1892: Nowaczyk and Antonow, 1997; ST: sediment traps location of Hebbeln (2000). (For interpretation of the references to colour in this figure legend, the reader is referred to the web version of this article.)

excursions (e.g., 9 kyr duration for the Laschamp in Nowaczyk and Baumann, 1992), and the apparent cumulative thickness of excursional zones reach up to almost 50% of the recovered sedimentary sequence (see Fig. 5 of Nowaczyk et al., 1994; and Fig. 3b in O'Regan et al., 2008). Fortuitous variations in sedimentation rate must be invoked to explain these amplified "excursions". Uncertainties in age control in Arctic sediments add to the freedom in labeling the Arctic excursions, and make it difficult to unequivocally correlate apparent excursions in the Arctic area to excursions documented elsewhere. Several supposed geomagnetic excursions such as the Norwegian–Greenland Sea excursion (Bleil and Gard, 1989; Nowaczyk and Baumann, 1992; Nowaczyk et al., 1994; Nowaczyk and Frederichs, 1999) and the Fram Strait excursion (Nowaczyk and Baumann, 1992) have not been observed elsewhere.

Studies on sediment cores HLY0503-06, 08, 10, 11, and 13, retrieved by the 2005 Healy-Oden Trans-Arctic Expedition (HOTRAX'05) from the Mendeleev–Alpha Ridge (Fig. 1), recognized titanomaghemite and titanomagnetite as magnetic remanence carriers (Channell and Xuan, 2009; Xuan and Channell, 2010). Thermal demagnetization of the natural remanences (NRM) indicated that low and negative NRM inclinations in these sediments are partially carried by titanomaghemite that could have formed during seafloor diagenetic oxidation from original titanomagnetite. These authors proposed that negative inclinations in cores from the Mendeleev–Alpha Ridge represent partially self-reversed chemical remanent magnetization (CRM). High Ti contents and high oxidation states indicated by the X-ray energy-dispersive spectroscopy (EDS) and X-ray diffraction (XRD) data suggest the conditions required for partial self-reversal by ionic reordering during diagenetic maghemitization. This process appears to have affected all HOTRAX'05 cores collected from the Mendeleev–Alpha Ridge (see Channell and Xuan, 2009; Xuan and Channell, 2010). The oxic diagenetic conditions in Arctic Ocean sediments were attributed to low concentrations of marine organic matter combined with low sedimentation rates, leading to minimal burial of deposited organic matter and low activity of the microbial reduction processes.

Whether paleomagnetic records from the Lomonosov Ridge and the Yermak Plateau represent genuine geomagnetic field behavior, or are due to a partial self-reversal process similar to that proposed for the Mendeleev–Alpha Ridge sediments, has important implications for the use of these paleomagnetic records for stratigraphy. In this paper, paleomagnetic and rock magnetic measurements as well as EDS, XRD, and textural analyses are employed to study HOTRAX'05 Core HLY0503-20JPC (hereafter referred to as Core 20) from the Lomonosov Ridge and HLY0503-22JPC (hereafter referred to as Core 22) from the Yermak Plateau (Fig. 1), to investigate the origin of negative NRM inclinations in these sediments and evaluate the regional importance of the partial self-reversal mechanism advocated for the Mendeleev–Alpha Ridge sediments.

2. Materials and methods

The 10.58-m long Core 20 was retrieved from an intra-ridge depression in the central Lomonosov Ridge at 88°48.36′N, 163°34.78′E, in 2654 m water depth (Fig. 1; Björk et al., 2007). Core 20 is mostly composed of interlaminated brown to dark brown and lighter colored yellowish (olive, grayish) brown silty clays, clays, and sandy clays, with occasional coarser ice rafted debris (IRD). Core 22 has a length of 13.31 m and was recovered on the Yermak Plateau at 80°29.39′N, 7°46.14′E, in 798 m water depth (Fig. 1). Core 22 mainly consists of grayish/greenish to dark grey silty clays. Where possible, the planktic foraminifera *Neogloboquadrina pachyderma* (sinistral) was picked from the 150–250 μm fraction in the top 5.85 m of Core 22 for oxygen isotope measurements. Planktic foraminifers from two samples from Core 22 at 1 m below seafloor (mbsf) and 1.38 mbsf were used for accelerator mass spectrometry (AMS) ^{14}C dating. Grain size (<2 mm) analyses were performed every 5 cm in the top 5.85 m of Core 22 using a Malvern Mastersizer 2000 laser particle analyzer after the bulk sediment was thoroughly dispersed using Na-metaphosphate (Darby et al., 2009).

U-channel samples were collected from working halves of Cores 20 and 22. The u-channel samples are enclosed in plastic containers with a 2 × 2 cm^2 cross-section and the same length as the core section (usually 150 cm), with a clip-on plastic lid that allows the samples to be sealed to retard dehydration and other chemical and physical alteration. The NRM of all u-channel samples was measured at 1-cm spacing before demagnetization and after alternating field (AF) demagnetization at 14 steps in the 10–100 mT peak field range, using a 2G Enterprises cryogenic magnetometer designed to measure u-channel samples. For each demagnetization step, samples from Core 20 were measured after two separate demagnetization sequences for the X, Y and Z sample axes to monitor any spurious anhysteretic remanence (ARM) acquisition during AF demagnetization. At each demagnetization step, the first XYZ demagnetization sequence was followed by measurement, and then the ZXY demagnetization sequence was followed by repeat measurement. As no discernable affect was observed with differing order of demagnetization, only the XYZ demagnetization sequence was applied to samples from Core 22. Magnetic susceptibility measurements were carried out using a susceptibility track designed for measuring u-channel samples (Thomas et al., 2003). ARM was acquired in a peak alternating field of 100 mT with a 50 μT DC bias field, and measured prior to demagnetization and after demagnetization at 9 steps in the 20–60 mT peak field range.

Eighty-nine bulk sediment samples were collected at 1–2 cm spacing from three intervals of Core 22 for hysteresis loop and backfield curve measurements using a Princeton Measurements Corp. vibrating sample magnetometer (VSM). Six of the bulk samples were also used for high-resolution first order reversal curve (FORC) measurements on a VSM. Discrete samples (~2 × 2 × 2 cm^3 each) were collected from Cores 20 and 22 in cubic plastic boxes alongside the u-channel samples. Magnetic susceptibility of the discrete samples was measured in 15 different directions using an AGICO KLY-3S susceptibility bridge for the determination of anisotropy of magnetic susceptibility. The discrete samples were then dried in a magnetically shielded space with flowing helium gas before being taken out from the plastic containers, and wrapped in Al foil for NRM measurements after thermal treatment in 25 °C steps in the 50–600 °C temperature range. Ten additional discrete samples (~2 × 2 × 2 cm^3 each) were sub-sampled from the u-channels of Cores 20 and 22, after u-channel measurements were completed. The samples were taken from intervals that are characterized by typical positive and negative AF-derived NRM inclinations. Samples were first dried and wrapped in Al foil in preparation for a three-orthogonal-axis isothermal remanent magnetization (IRM) thermal demagnetization experiment, following the method of Lowrie (1990). IRM was acquired in DC fields of 1.2 T, 0.5 T, and 0.1 T sequentially along three orthogonal axes of the samples, and then the composite IRM was measured before the thermal treatment and after thermal treatments in 25 °C steps in the 50–600 °C temperature range.

Magnetic extracts were made using bulk sediments from the 0.91–1.02 m, 3.64–3.74 m, 3.93–4.05 m, and 4.86–4.97 m depth intervals of Core 20, and from the 0.67–0.77 m, 1.01–1.13 m, 1.93–2.06 m, and 3.43–3.55 m depth intervals of Core 22, following the extraction procedures described in Xuan and Channell (2010). A proportion of the magnetic extract samples were used for IRM acquisition experiments on a Princeton Measurements Corp. alternating gradient magnetometer (AGM). IRM of the extracts was measured at one hundred equidistant field steps on a logarithmic scale ranging from ~7 mT to 1 T. Selected magnetic extracts were spread on a carbon tape and examined under a Zeiss EVO scanning electron microscopy (SEM) equipped with Genesis EDS. Elemental maps were collected on micron-sized grain clusters in the extract samples for up to 20 h using the EDS. XRD analyses were performed on the magnetic extracts using a Rigaku Ultima IV X-ray diffractometer. The extracts were placed on a zero background sample holder, and diffraction patterns were collected within four 2θ intervals (i.e., 29–31°, 34–37°, 42–44.5°, 52–65°) that cover the dominant peaks of standard magnetite and titanomaghemite associated with the [2 2 0], [3 1 1], [4 0 0], [4 2 2], [5 1 1], and [4 4 0] diffraction planes. A 0.01° step-size and a 20-s count-time were used for the analyses. Susceptibility of the magnetic extract samples were monitored on heating from room temperature to 700 °C and subsequent cooling to room temperature, in an argon gas environment, using a KLY-3S susceptibility bridge. For two extract samples from Core 20 (from 0.91–1.02 m and 4.86–4.97 m depth intervals), second heating and cooling curves were measured after the samples had been heated 700 °C and cooled to room temperature.

3. Results

3.1. Natural remanent magnetization

U-channel NRM measurements of Cores 20 and 22, usually reveal characteristic components after 20–30 mT peak field AF demagnetization. Component declination and inclination, with maximum angular deviation (MAD) values, were calculated for the 20–80 mT demagnetization peak field range for both cores, using the principal component analysis method (Kirschvink, 1980) and the UPmag software (Xuan and Channell, 2009). For Core 20 from the Lomonosov Ridge, MAD values are generally around 10°, indicating that the NRM component directions are reasonably well defined (Fig. 2). The NRM inclination record of Core 20 is characterized by several thick (up to ~50 cm) intervals of shallow/negative inclination in the top 10 m of the core, with the first significant inclination drop occurring at ~3.4 mbsf. In addition, component NRM inclinations of Core 20 are generally tens of degrees lower than the expected inclination (vertical green line in Fig. 2) for a geocentric axial dipole (GAD) field at the core location. There are no significant differences in component directions calculated using data from the XYZ (blue lines in Fig. 2) and the ZXY (red lines in Fig. 2) demagnetization sequences. Therefore, shallow/negative NRM inclinations are not caused by spurious ARM acquisition during AF demagnetization. These observations are very similar to those of the Mendeleev–Alpha Ridge cores studied by Channell and Xuan (2009), and by Xuan and Channell (2010). For Core 22 from the Yermak Plateau, MAD values associated with the component directions are mostly less than 5° (Fig. 2), which is markedly lower than that of Core 20 and the Mendeleev–Alpha Ridge cores. Component NRM inclinations of Core 22 appear to be less shifted from the expected GAD value. Four ~10–30 cm thick shallow/negative inclination intervals can be observed in the top 6 mbsf at ~1 mbsf, ~2 mbsf, ~3.5 mbsf, and ~5.5 mbsf of Core 22 (Fig. 2).

Thermal demagnetization of the NRM of Cores 20 and 22 show behavior comparable to the AF demagnetization of NRM (Fig. 3), with characteristic components generally revealed after 50–175 °C thermal treatments. Thermal demagnetization data often show hints of overlapping components at high temperature steps (300–600 °C) for samples that have either negative (e.g., Core 22 1.98 m, Core 20 7.62 m) or shallow positive (e.g., Core 22 2.15 m) AF-derived NRM inclinations. Furthermore, NRM intensities monitored during thermal demagnetization (lower plots in Fig. 3) clearly show that the negative inclination or shallow positive inclination components are often largely unblocked below ~300 °C. These

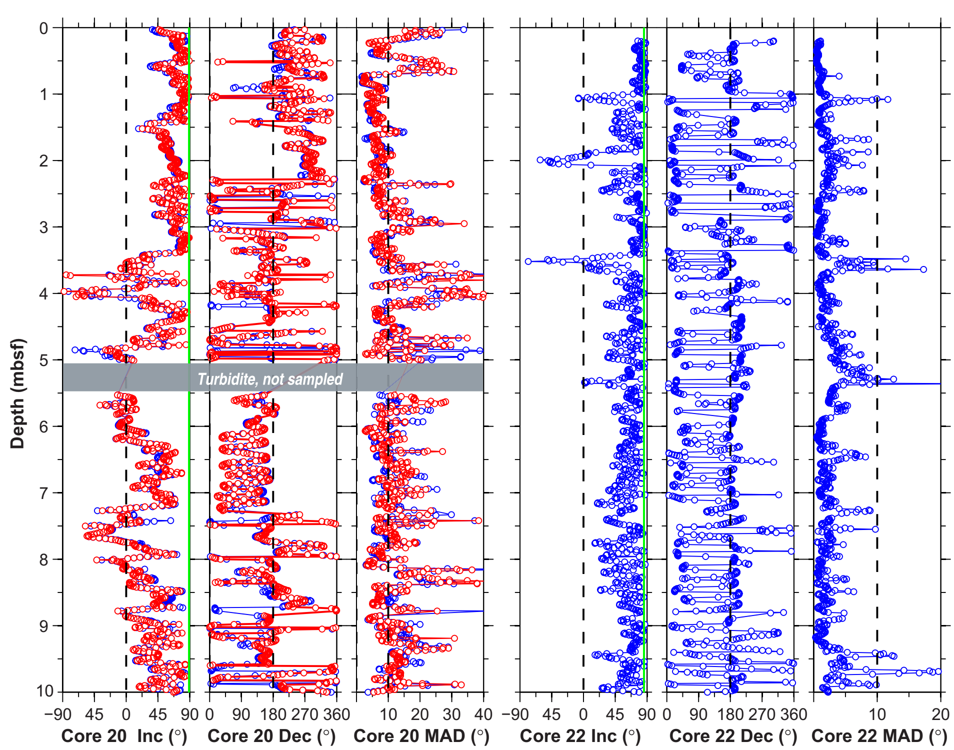

Fig. 2. Component inclination and declination with maximum angular deviation (MAD) calculated for the 20–80 mT peak alternating field range for Cores 20 (Lomonosov Ridge) and 22 (Yermak Plateau). Results calculated using data from XYZ and ZXY demagnetization sequences, for the three sample axes, are in blue and red, respectively. Note that Core 22 samples were measured using only the XYZ demagnetization sequence. Declination values are arbitrary as cores were not oriented in azimuth. (For interpretation of the references to colour in this figure legend, the reader is referred to the web version of this article.)

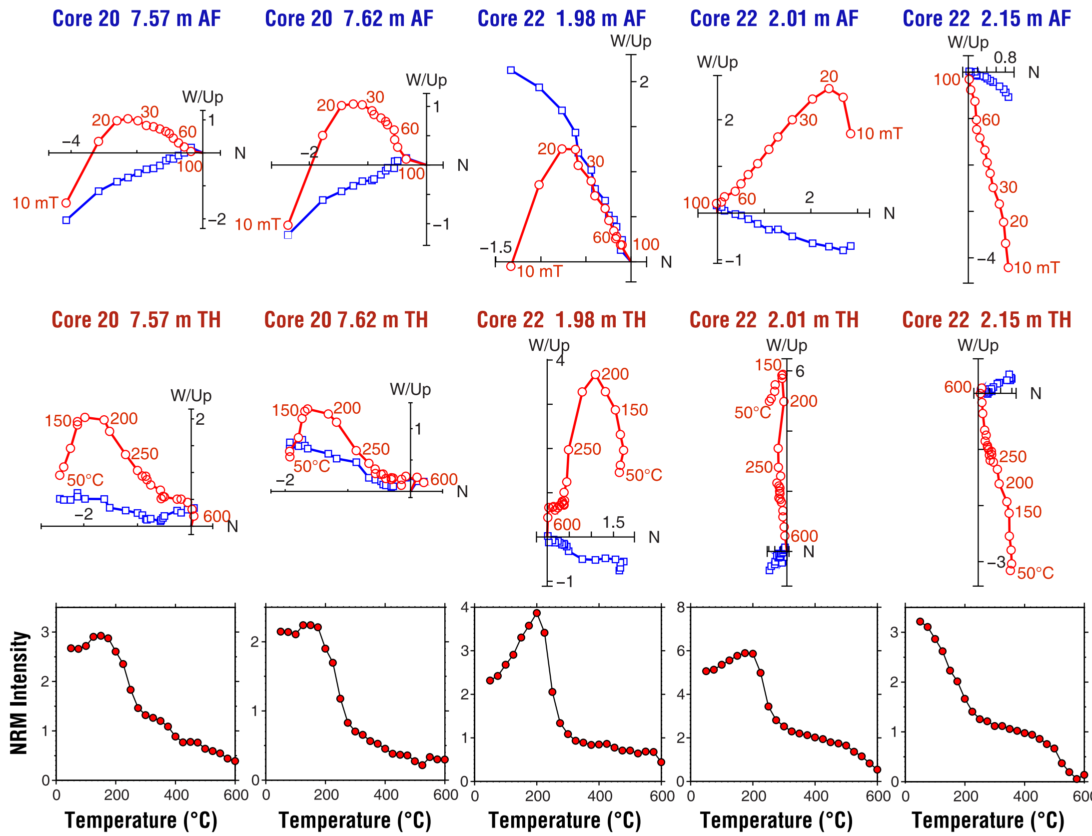

Fig. 3. Orthogonal projection of thermal demagnetization data for discrete cubic (~2 × 2 × 2 cm^3) samples from Cores 20 and 22, compared to orthogonal projection of alternating field demagnetization data for u-channel intervals from the same depth level, with NRM intensity variations during thermal demagnetization displayed on the bottom. Peak demagnetizing field ranges are 10–60 mT in 5 mT steps then 60–100 mT in 10 mT steps. Temperature ranges are 50–600 °C in 25 °C steps for all samples. Circles (red) and squares (blue) denote projection on vertical and horizontal planes, respectively. Declination values are arbitrary as cores were not oriented in azimuth. Meter levels correspond to meters below seafloor (mbsf) of each core as in Fig. 2. Unit for intensity scale is mA/m. (For interpretation of the references to colour in this figure legend, the reader is referred to the web version of this article.)

observations indicate that shallow/negative inclinations in Cores 20 and 22 are carried by a magnetic phase that has unblocking temperatures largely below ~300 °C. Similar results were reported by Channell and Xuan (2009), and by Xuan and Channell (2010) for the Mendeleev–Alpha Ridge cores, in which shallow/negative NRM inclinations were attributed to the influence of a self-reversed CRM carried by diagenetic titanomaghemite that has "unblocking" temperatures (due to inversion) largely below ~300 °C.

3.2. Magnetic grain size in Core 22

The magnetic grain-size proxy κ_{ARM}/κ was calculated for Core 22 using u-channel ARM (after 35 mT demagnetization) and susceptibility measurements (Fig. 4A). Because ARM is mainly carried by smaller (single domain to pseudo-single domain) magnetic particles, typically sub-micron to few microns in size, whereas susceptibility is linked more to larger (multi-domain) particles, higher values of κ_{ARM}/κ indicate finer grains of magnetite (see King et al., 1983). Hysteresis parameters of the 89 bulk samples (purple circles in Fig. 4A), estimated from the hysteresis loop and backfield curve measurements, are grouped in the pseudo-single (PSD) domain field when plotted on a Day et al. (1977) hysteresis ratio plot (Fig. 4B). Apparently, samples with higher κ_{ARM}/κ values (blue circles in Fig. 4B) indicate finer magnetic grains on the Day plot than samples with lower κ_{ARM}/κ values (yellow circles in Fig. 4B), supporting κ_{ARM}/κ as a magnetic grain size proxy. In addition, first order reversal curve (FORC) diagrams of samples with decreasing κ_{ARM}/κ values, processed using the FORCinel (Harrison and Feinberg, 2008) software with a smoothing factor of 8, show decreasing coercivities and increasing interactions that are consistent with increasing magnetic grain sizes (Fig. 4C). According to the King et al. (1983) calibration, κ_{ARM}/κ values of Core 22 imply magnetic grain sizes in the 0.1–20 μm range (Fig. 5A). The κ_{ARM}/κ data of Core 22 were compared to variations of population in each physical grain size bin analyzed by the Malvern Mastersizer 2000 laser particle analyzer. The best correlation, with a correlation coefficient of 0.64 (Fig. 5B and C), was found between the κ_{ARM}/κ and the grain bin with a center size of ~10.66–11.25 μm (light blue closed circles in Fig. 4). Physical grain size distributions of samples with typical high and low κ_{ARM}/κ values clearly indicate larger physical grain sizes for lower κ_{ARM}/κ value samples (Fig. 5D), suggesting that κ_{ARM}/κ represents physical grain size variation in Core 22. Mean size of sortable silt was estimated using the 10–63 μm grains, although the 10 μm lower end of the sortable silt typically determined by sedigraph data may correspond to 6–8 μm on laser analyzer scale depending on mica content in the sediments (e.g., McCave et al., 2006). The calculated sortable silt mean size variation appears to track the volume percentage change of the sortable silt, and shows inverse relationship with abundance of the ~10.66–11.25 μm grains (Fig. 4). Mean size of the sortable silt correlates with κ_{ARM}/κ data in general with coarser (finer) grains corresponding to smaller (larger) values of κ_{ARM}/κ. The lack of correlation between κ_{ARM}/κ and population of coarse (>63 μm) grains (Fig. 4A, and Fig. 5B) indicates that κ_{ARM}/κ variations are not caused by IRD input.

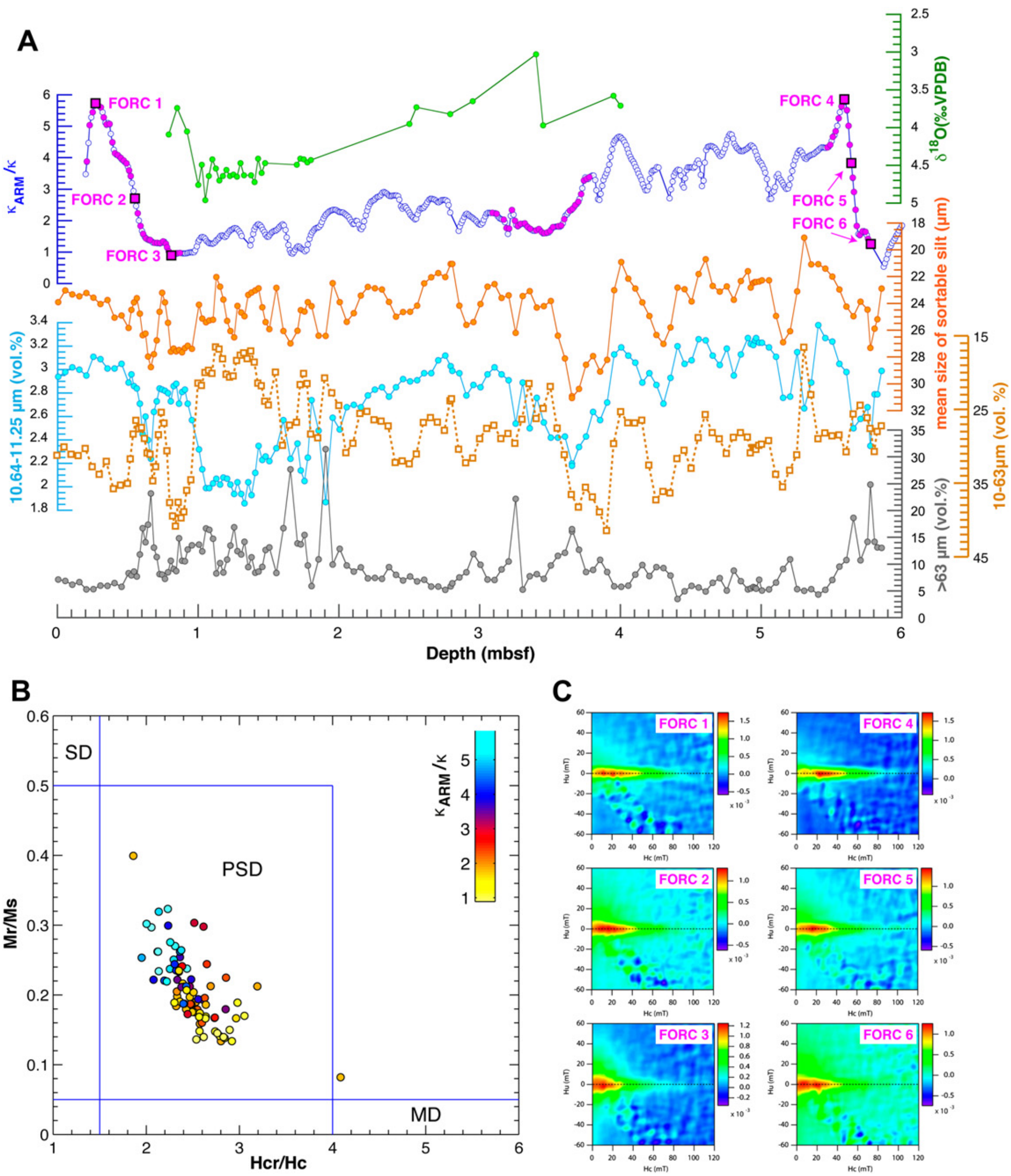

Fig. 4. A) Core 22 κ_{ARM}/κ (blue open circles), planktic $\delta^{18}O$ (green circles), sortable silt (10–63 μm) mean size (orange circles), and population variations of the 10.64–11.25 μm (light blue circles), 10–63 μm (orange squares) and >63 μm size grains (gray circles); note that *y* axes of the mean size and volume percentage data of sortable silt are reversed for comparison purpose; B) magnetic hysteresis ratios of samples collected from three intervals of Core 22 (purple circles in A) that capture dramatic changes in either κ_{ARM}/κ or the NRM inclination record; and C) FORC diagrams of six representative samples (purple squares in A) from the two intervals of abrupt change in κ_{ARM}/κ. Sample data points in B) were colored according to their corresponding κ_{ARM}/κ values. (For interpretation of the references to colour in this figure legend, the reader is referred to the web version of this article.)

3.3. Age constraints

Ages of sediments from the central Lomonosov Ridge have been primarily provided by correlation of sediment color, density, and ARM/IRM cycles to $\delta^{18}O$ reference curves (Jakobsson et al., 2000; O'Regan et al., 2008), corroborated by optically stimulated luminescence dating (Jakobsson et al., 2003) as well as sporadic biostratigraphic markers such as coccolithophorid *E. huxleyi* that has late Brunhes age (Backman et al., 2004). Such age estimates yield 1–2 cm/kyr average sedimentation rates for cores from the intra-ridge depression in the central Lomonosov Ridge with apparently continuous deposition during the late Brunhes. This is consistent with the long-term (last 17 Myr) ~1.5 cm/kyr average sedimentation rates derived from a $^{10}Be/^{9}Be$ age model for the ACEX core (Backman et al., 2008; Frank et al., 2008). Using bulk density and magnetic susceptibility logs, Sellén et al. (2010) correlated Core 20 to other cores from the central Lomonosov Ridge (Fig. 6 of Sellén et al., 2010). The authors recognized four stratigraphic horizons in the top ~6.5 m of Core 20 that can be tied to ACEX, PS 2185, 96/12-1 PC, and HLY0503-18JPC, although Core 20 appears to have a somewhat more complicated stratigraphy due to additional sediment intercalations. According to this correlation and age models established for the other Lomonosov Ridge cores (Jakobsson et al., 2001; Spielhagen et al., 2004; O'Regan et al.,

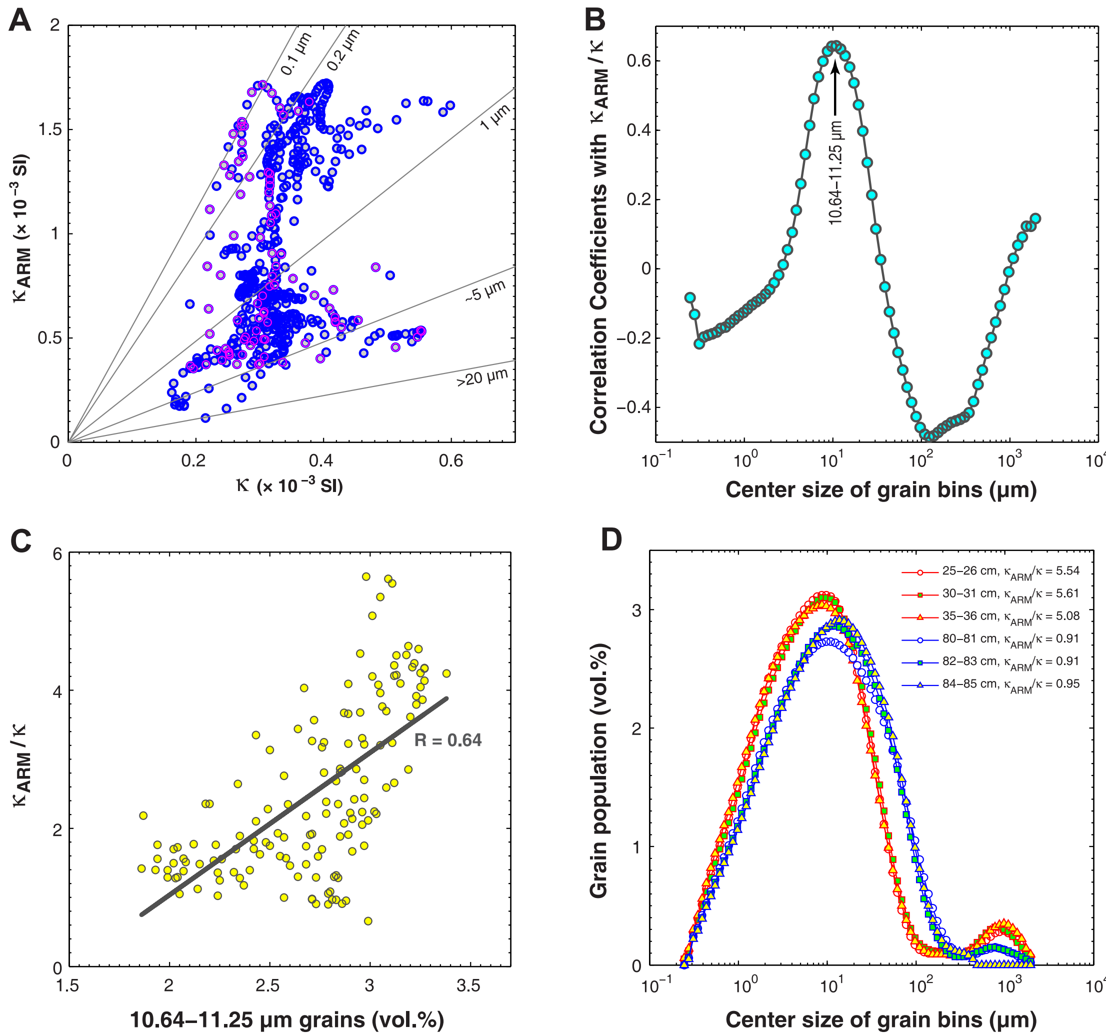

Fig. 5. A) Core 22 κ_{ARM} versus κ plot, with magnetic grain sizes marked according to the King et al. (1983) calibration, purple circles denote samples from intervals where hysteresis ratios were also measured in Fig. 4B; B) correlation coefficients between κ_{ARM}/κ and variation in each physical grain size bin population; C) κ_{ARM}/κ plotted against populations of the 10.64–11.25 μm size grains in Core 22, with the least square fit line of the data showing in dark gray; D) physical grain size distributions of samples with typical high (red lines) and low (blue lines) κ_{ARM}/κ values. (For interpretation of the references to colour in this figure legend, the reader is referred to the web version of this article.)

2008), it is reasonable to expect most of Core 20 to have been deposited in the Brunhes Chron, restricting the low/negative inclinations in the upper part of the core to Brunhes-aged magnetic excursions or to distortions of the paleomagnetic record. NRM component inclinations from Core 20 appear to be comparable to inclinations observed in nearby cores including Core 96/12-1 (Fig. 3 of Jakobsson et al., 2000), Core 2185 (Fig. 3 of Spielhagen et al., 2004), and ACEX (Fig. 3 of O'Regan et al., 2008). The first apparent drop in the AF-derived NRM inclination at ~3.4 mbsf in Core 20 is observed at a similar depth (~4.5 rmcd) in ACEX and other Lomonosov Ridge cores, and was interpreted as the Biwa II excursion with an assumed age of ~240 ka (Jakobsson et al., 2000; O'Regan et al., 2008).

The κ_{ARM}/κ curve of Core 22 clearly resembles the global benthic oxygen isotope record, with finer grains (larger κ_{ARM}/κ) occurring in interglacial, high sea level intervals (Fig. 4A). For instance, the κ_{ARM}/κ peak intervals at ~0.25 mbsf and ~5.6 mbsf could be correlated to late Holocene and MIS 5e, respectively. Only limited intervals of Core 22 yield sufficient foraminifera (5–10) for stable oxygen isotope measurements (green circles in Fig. 4A). The $\delta^{18}O$ values from those intervals typically range between 3 and 5‰ VPDB, with a trend of increasing values from the Holocene towards the last glacial (MIS 2) and then decreasing values towards the last interglacial, thus covarying with the κ_{ARM}/κ data. Similar co-variation of the κ_{ARM}/κ and $\delta^{18}O$ can be observed in a wider stratigraphic interval in nearby cores 1533 (Nowaczyk et al., 1994) and 2138 (Nowaczyk and Knies, 2000) (Fig. 6). A lag of several tens of centimeters between the $\delta^{18}O$ and the κ_{ARM}/κ curves in the deglaciation interval (Fig. 6) is probably related to local $\delta^{18}O$ depletion in surface waters caused by the early deglaciation of the Svalbard/Barents Ice Sheet (e.g., Knies et al., 1999). Comparison of κ_{ARM}/κ data from Core 22 with that from Cores 1533 and 2138, dated using oxygen isotope stratigraphy and radiocarbon ages appears to constrain the top ~6 m of Core 22 to MIS 1–6 (Fig. 6). This age model is corroborated by two AMS ^{14}C datings from 1 mbsf and 1.38 mbsf in Core 22 yielding ^{14}C ages of 15.34 ka and 18.50 ka, respectively. Using the reservoir age of 440 years and the same calibration to calendar years as in Nowaczyk et al. (2003), we obtain calibrated ages of 17.71 ka and 21.35 ka for the two dated samples (yellow triangles on leftmost plot in Fig. 6). A tentative age model for Core 22 was constructed by correlating features (green circles in Fig. 7) in κ_{ARM}/κ curve to the PISO-1500 oxygen isotope stack record (Channell et al., 2009) for the last ~160 kyr, with additional tie points provided by the two AMS ^{14}C dates (yellow circles in Fig. 7).

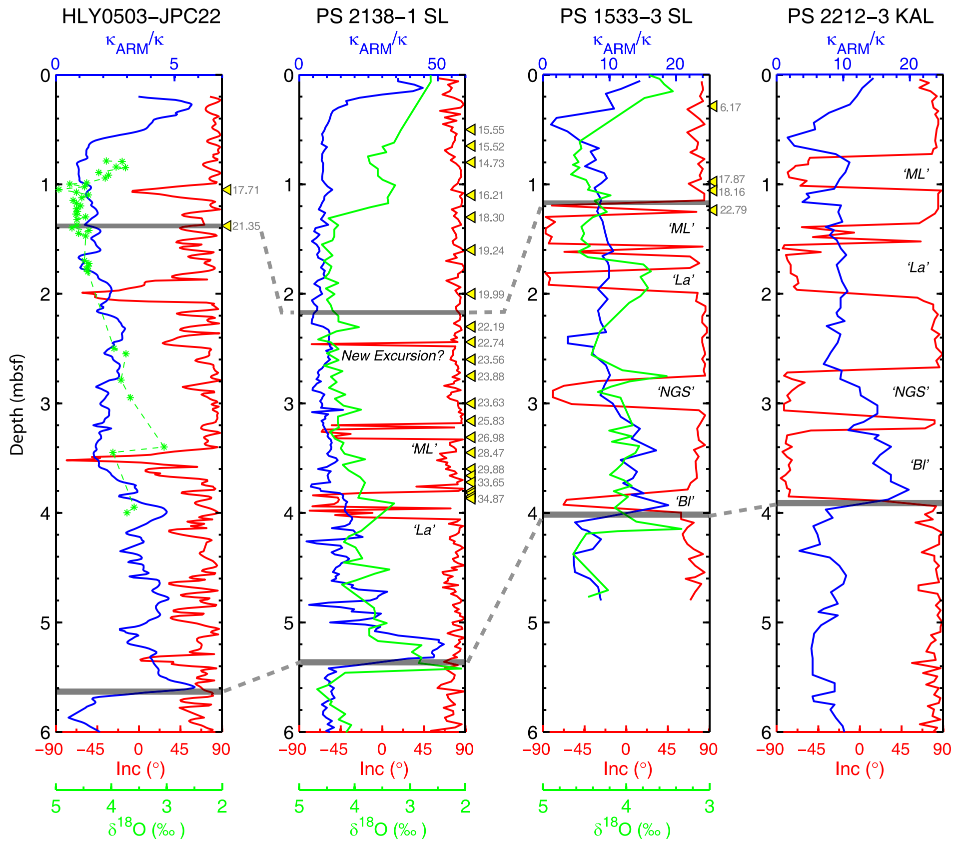

Fig. 6. NRM inclination, κ_{ARM}/κ, $\delta^{18}O$, and calibrated ^{14}C ages from Core 22 compared to other cores from the Yermak Plateau: Core PS 2138 (Nowaczyk and Knies, 2000; Nowaczyk et al., 2003), Cores PS 1533 and PS 2212 (Nowaczyk et al., 1994). Grey lines show correlation of the inferred MIS 5/6 boundary (abrupt increase in κ_{ARM}/κ at ~4–5.8 m) and of the older ^{14}C age in Core 22 at the Last Glacial Maximum.

According to the age model, accumulation rates of Core 22 sediments vary in the ~2–8 cm/kyr range during the last ~160 kyr (Fig. 7). The four shallow/negative inclination intervals in Core 22 are constrained in this age model to the last ~130 kyrs, and the shallow/negative inclination intervals appear to occur close to paleointensity minima in the PISO-1500 paleointensity stack (Fig. 7).

3.4. Magnetic fabric of sediments

The statistical orientation of magnetic grains in sediments can generate anisotropy of the magnetic susceptibility (e.g., Hamilton and Rees, 1970; Rochette et al., 1992). A typical "sedimentary fabric" comprises principal axis (K_{max} K_{int} K_{min}) of a susceptibility ellipsoid oriented with K_{min} vertical, and K_{max} and K_{int} dispersed in the horizontal plane. Anisotropy tensors of Core 20 and 22 samples were calculated using the AGICO software that is based on statistics from Jelínek and Kropáček (1978). For 51 samples from Core 20, mean and standard deviation (σ) of K_{max}, K_{int}, and K_{min} yielded values of 1.018 (σ: 0.005), 1.008 (σ: 0.004), and 0.974 (σ: 0.008), respectively. Mean and standard deviation of K_{max}, K_{int}, and K_{min} for 71 samples from Core 22 are 1.016 (σ: 0.006), 1.007 (σ: 0.004), and 0.977 (σ: 0.008), respectively. Degrees of anisotropy ($100 \times (K_{max} - K_{min})/K_{max}$) for both cores are relatively low, with values of ~4 and ~3 for Core 20 and Core 22, respectively. The sediments are characterized by an oblate ellipsoid representing a rather typical sedimentary fabric, with mean $K_{max} \times K_{min}/K_{int}^2$ values of 0.97 for Core 20 and 0.986 for Core 22. K_{max} and K_{int} axes in both Cores 20 and 22 seem to have similar preferred orientations on the horizontal plane (Fig. 8). As both cores were not oriented in azimuth, the similarity in preferred orientations of K_{max} and K_{int} in the two cores implies that this preferred orientation was imposed during sampling (see e.g., Gravenor et al., 1984). Similar observations were made by Løvlie et al. (1986) for Yermak Plateau cores, and were interpreted as a secondary magnetic fabric induced during the sub-sampling procedure. Nowaczyk et al. (2003) attributed similar results in Fram Strait core PS1535 (Fig. 1) to a numerical artifact of the applied software. The K_{min} directions of samples from both cores are almost perpendicular to the bedding plane (Fig. 8), with mean K_{min} inclinations of 86.5° and 86.2° for Cores 20 and 22 respectively, indicating typical sedimentary fabrics, precluding the possibility that shallow NRM inclinations were caused by anomalous magnetic fabric in these sediments.

3.5. Magnetic mineralogy

Thermal demagnetization of the three-orthogonal-axis IRM (Fig. 9) shows that samples from both Core 20 (in red) and 22 (in blue) are dominated by soft (<0.1 T) and medium (0.1–0.5 T) coercivity magnetic phases. The abrupt decreases in IRM intensity below ~300 °C, are attributed to the inversion of titanomaghemite. The decrease is manifest in the soft IRM, and even more so in the medium coercivity IRM, indicating that the titanomaghemite grains have a range of coercivities presumably due to variations in grain size and/or oxidation states. Difference between samples from intervals of typical positive and negative AF-derived NRM inclinations is not apparent in either core. This is probably because samples from positive (usually shallow) and negative inclination intervals have all been subjected to diagenetic maghemitization. The NRM inclination of a sample depends not only on the

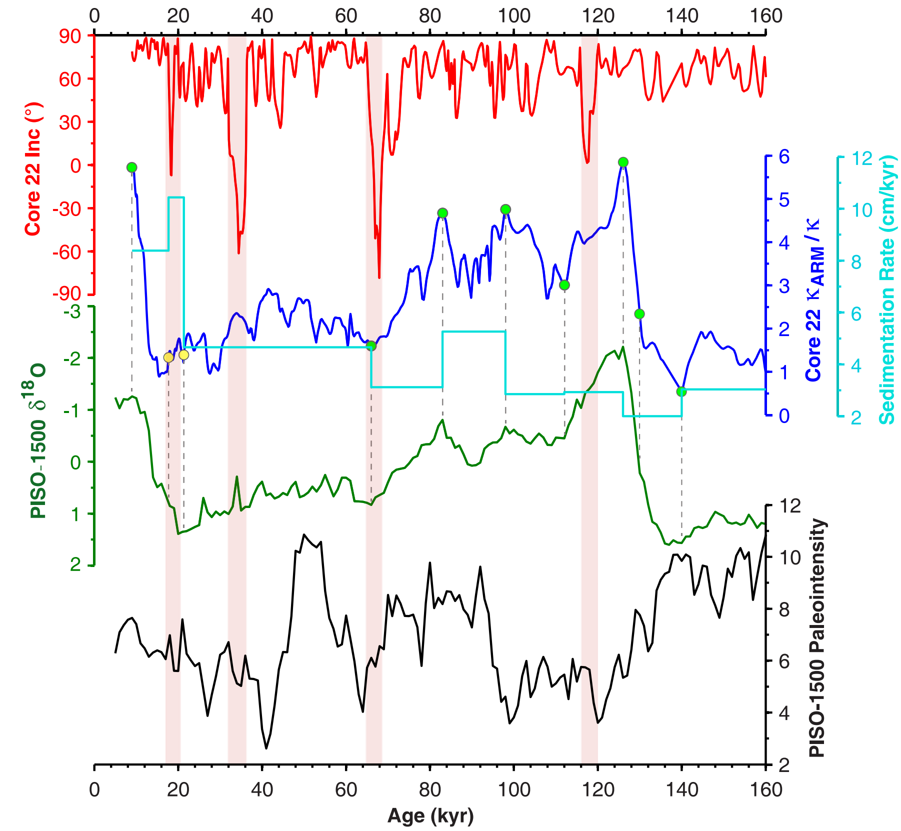

Fig. 7. Component inclination (red line) and κ_{ARM}/κ (blue line) data from Core 22 compared to PISO-1500 oxygen isotope (green line) and relative paleointensity (black line) stack records (Channell et al., 2009) for the last ~160 kyr. Core 22 κ_{ARM}/κ record was correlated to PISO-1500 oxygen isotope stack record using tie points marked as green circles as well as the two radiocarbon dates (yellow circles). Sedimentation rates between the age-model tie points are also shown (light blue lines). (For interpretation of the references to colour in this figure legend, the reader is referred to the web version of this article.)

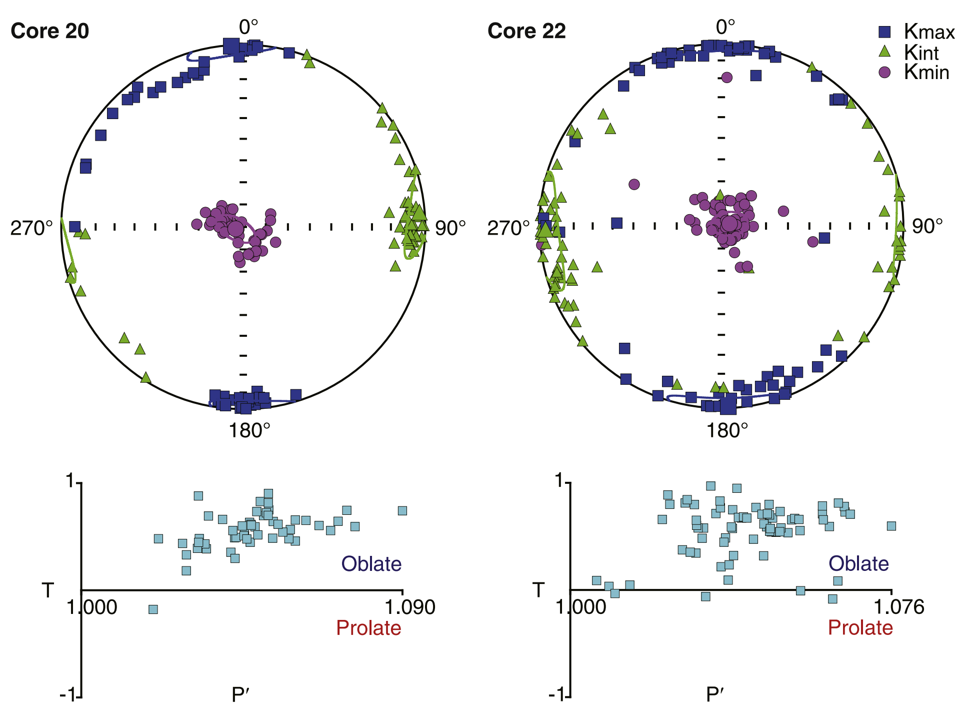

Fig. 8. Results of the analysis of anisotropy of magnetic susceptibility for 51 samples from Core 20, and 71 samples from Core 22. Top plots: Orientations of the principle axes K_{max}, K_{int}, and K_{min} for samples from Core 20 (left) and Core 22 (right). Mean directions (larger symbols) of K_{max}, K_{int}, K_{min}, and their 95% confidence ellipses (colored solid lines) are also shown. Bottom plots: corrected anisotropy degree P′ against shape parameter T (see Jelínek and Kropáček, 1978) showing oblate ellipsoids (with K_{min} vertical) indicating a typical sedimentary fabric for samples from both cores.

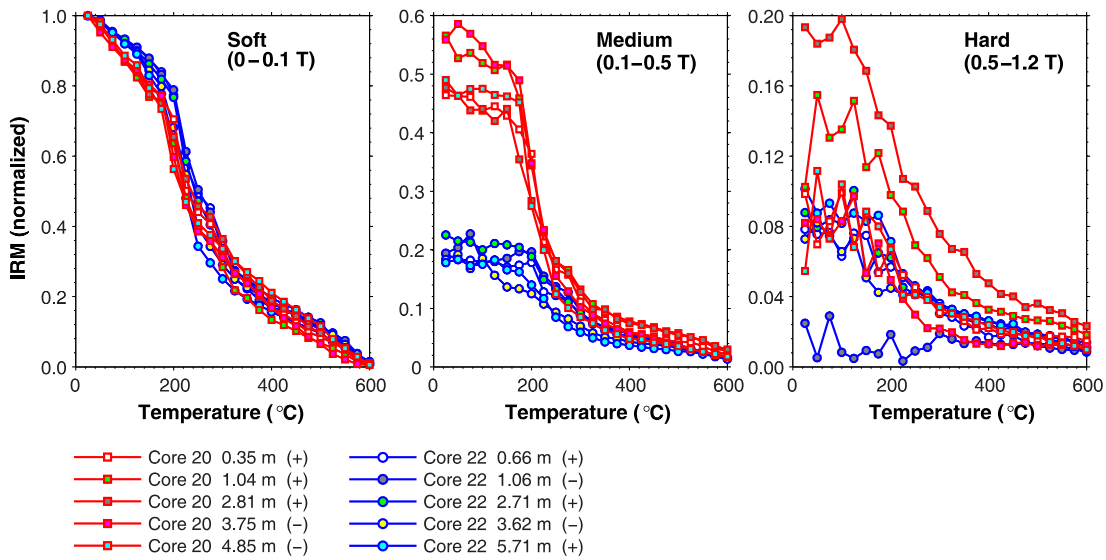

Fig. 9. Thermal demagnetization of three-axis isothermal remanent magnetizations (IRM) imposed orthogonally and sequentially in DC fields of 1.2 T (hard), 0.5 T (medium) and 0.1 T (soft), for samples collected from intervals showing positive (+) and negative (−) component AF-derived NRM inclinations in Cores 20 (red lines) and 22 (blue lines). IRM values of each sample were normalized by the room temperature soft component IRM. (For interpretation of the references to colour in this figure legend, the reader is referred to the web version of this article.)

proportion of grains that have undergone oxidation (and distortion of the NRM directions), but also on the oxidation state of the grains and on the statistical alignment achieved during acquisition of detrital remanent magnetization (DRM). On the other hand, samples from Core 20 (in red) clearly have higher proportion of the medium coercivity magnetic phase (Fig. 9), and therefore more titanomaghemite grains, than Core 22 samples (in blue). This observation is consistent with the fact that component inclinations of Core 22 appear to be less shifted from the expected geocentric dipole field value than those of Core 20, and MAD values associated with component directions from Core 22 are clearly smaller than those from Core 20 (see Fig. 2).

IRM acquisition data for magnetic extracts from Cores 20 and 22, plotted on logarithmic scale, are distinct from one another (top plot in Fig. 10), indicating different magnetic contents in sediments from the two cores. Similar to the Mendeleev–Alpha Ridge cores studied by Xuan and Channell (2010), the gradient of the IRM acquisition data of Core 20 magnetic extracts shows apparent asymmetry in shape, and satisfactory fits were achieved by modeling the IRM gradient data using two magnetic coercivity components (method of Heslop et al., 2002). Results from three magnetic extract samples of Core 20 are very similar to one another (middle plots in Fig. 10), yielding mean coercivities of ~55 mT and ~108 mT for the two magnetic components, consistent with the presence of titanomagnetite and titanomaghemite, respectively. As discussed by Xuan and Channell (2010), coercivities of titanomaghemite are expected to be slightly higher than those of titanomagnetite. For Core 22 magnetic extracts, the gradients of the IRM data show less asymmetry (bottom plots in Fig. 10). Reasonable fits are obtained by modeling the IRM gradient data using one magnetic coercivity component with mean coercivity of ~32 mT, although small mismatches are observed between the IRM gradient data and the fitting curves. The results are repeatable for magnetic extracts from the three dominantly negative inclination intervals in the top 4 m of Core 22 (bottom plots in Fig. 10).

Susceptibility of eight magnetic extract samples from Cores 20 and 22, monitored on heating from room temperature to 700 °C, show broad peaks or humps at around 300 °C followed by an abrupt drop in susceptibility at higher temperatures (red curves in Fig. 11A and B). These features are however not observed in susceptibility measured during subsequent cooling from 700 °C to room temperature (blue curves in Fig. 11A and B). The humps are probably related to titanomaghemite inversion, although unblocking of very fine magnetite grains that are in a single domain (SD) state at room temperature but pass through the SD to superparamagnetic transition during heating, may have contributed to the humps in the susceptibility curves (e.g., Wang and Løvlie, 2008). Titanomaghemite when heated to 600 °C typically leads to intergrowths of minerals including magnetite and ilmenite without substantial increase in susceptibility, thereby explaining the absence of ‘humps’ in the cooling curves. In addition, the humps are not seen in repeated heating and cooling curves of susceptibility measured for two magnetic extract samples from Core 20 that had been heated up to 700 °C and cooled to room temperature (Fig. 11C). The repeated heating and cooling curves of the two samples show typical magnetite behaviors and seem to be reversible (Fig. 11C), consistent with magnetite being the magnetic inversion product from titanomaghemite during the first heating and cooling of the samples. The cooling curves are generally below the heating curves possibly because some of the very fine grain magnetites have been oxidized to hematite during heating at high temperatures. The other observation from the high temperature susceptibility data (Fig. 11A and B) is that the humps in the heating curves appear to be more apparent in Core 20, indicating a higher proportion of titanomaghemite in this core. This is consistent with the three-orthogonal-axis IRM thermal demagnetization data and apparent absence of asymmetry in the IRM gradient data for Core 22 magnetic extracts.

3.6. EDS and XRD analyses

From EDS observations, the total image spectra of magnetic extract samples from Cores 20 and 22, collected during the elemental mapping, are comparable to each other with dominant peaks for O, Ti, and Fe (Fig. 12). The elemental maps clearly show a number of grains that are rich in O, Ti, and Fe, consistent with the presence of titanomagnetite and/or titanomaghemite in these two cores. Assuming the observed grains are single phase titanomagnetite or titanomaghemite, Ti compositions (x) of the titanomagnetite or titanomaghemite were estimated using the simple

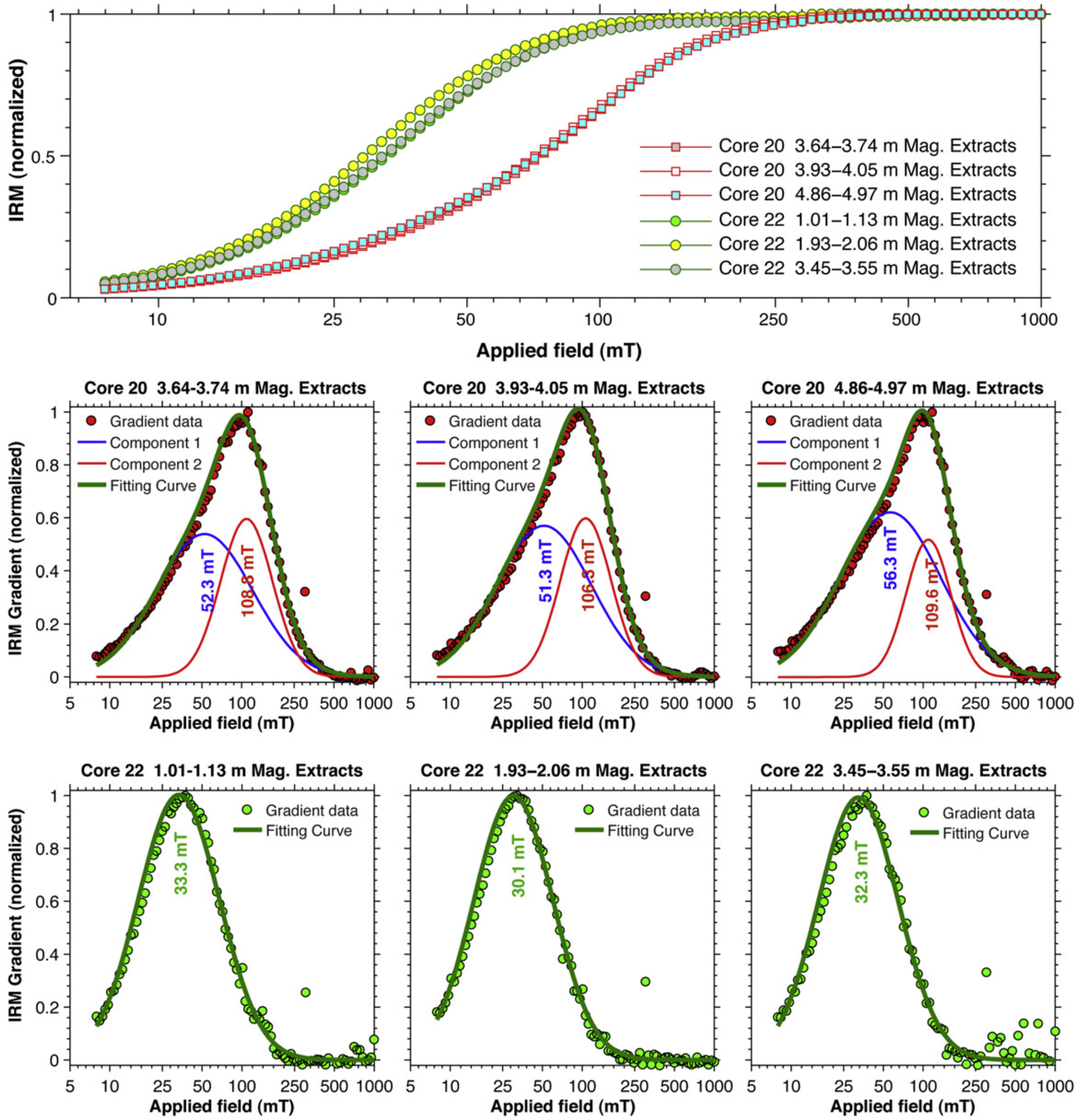

Fig. 10. IRM acquisition data for magnetic extracts from Cores 20 (squares linked with red lines) and 22 (circles linked with green lines), and two-component and one-component modeling of the IRM gradient data for magnetic extracts from Cores 20 (middle plots) and 22 (bottom plots), respectively. (For interpretation of the references to colour in this figure legend, the reader is referred to the web version of this article.)

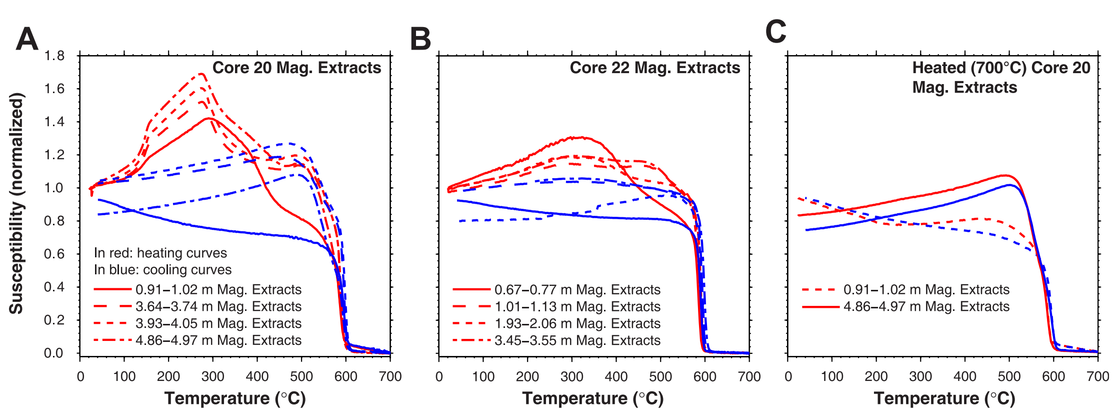

Fig. 11. Susceptibility monitored on heating from room temperature to 700 °C and subsequent cooling to room temperature, in an argon gas environment, for magnetic extracts from A) Core 22JPC and B) Core 20JPC; and C) repeated heating and cooling for magnetic extracts from 20JPC 0.9–1.02 m and 4.86–4.97 m. Heating (cooling) curves are in red (blue). (For interpretation of the references to colour in this figure legend, the reader is referred to the web version of this article.)

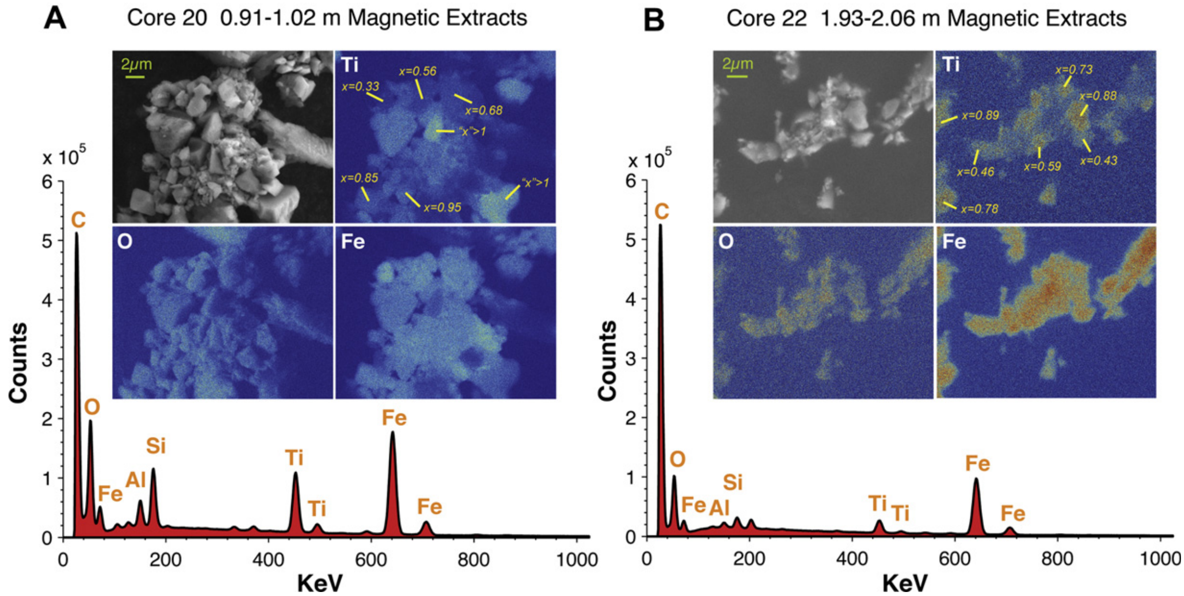

Fig. 12. SEM and EDS analyses for micron-sized grains of magnetic extracts from A) Core 20 and B) Core 22. The image comprises (titano)magnetite and/or titanomaghemite grains with various Ti contents with x values up to >0.9. The total image spectrum acquired during the mapping is also displayed, where the carbon peak is attributed to the carbon tape background.

equation: $x = 3/(1 + (Fe/Ti))$, where Fe/Ti is the atomic ratio estimated from the EDS data (see Doubrovine and Tarduno, 2006). The Ti composition varies widely from one grain to another, with calculated x values ranging from 0.33 to 0.95 for Core 20 extract (Fig. 12A), and from 0.43 to 0.89 for Core 22 extract (Fig. 12B).

XRD data of magnetic extract samples from Core 20 show two distinct peaks that fit magnetite and titanomaghemite for each of the six diffraction planes (Fig. 13). For magnetic extract samples from Core 22, the diffraction patterns are dominated by peaks consistent with magnetite. Titanomaghemite peaks are not apparent in the diffraction data from Core 22 magnetic extracts (Fig. 13). 2θ values and the estimated lattice parameters of the (titano)magnetite and titanomaghemite peaks on the six dominant diffraction planes are listed in Table 1. Core 20 magnetic extracts have mean lattice parameters of ~8.3907 to 8.3926 Å for the (titano)magnetite component, smaller than the mean values of ~8.3963 to 8.3969 Å of Core 22 magnetic extracts, presumably due to higher oxidation states of samples from Core 20. The titanomaghemite component in Core 20 magnetic extracts have mean lattice parameters of ~8.3543 to 8.3589 (Å) that are smaller than that (8.3647 Å) of magnetic extracts from the Mendeleev–Alpha Ridge Core 8 (see Xuan and Channell, 2010). According to Readman and O'Reilly (1972) and Nishitani and Kono (1983), these lattice parameters for the titanomaghemite component are sufficiently low that the oxidation states (z) must be >0.9 for a wide range of Ti contents or x values. These XRD data demonstrate that there is less titanomaghemite in Core 22, possibly due to a lower degree of diagenetic oxidation.

4. Discussion and conclusion

From the above analyses, it is clear that bulk samples or magnetic extracts of sediments from the Lomonosov Ridge Core 20 show rock magnetic properties comparable to that of the

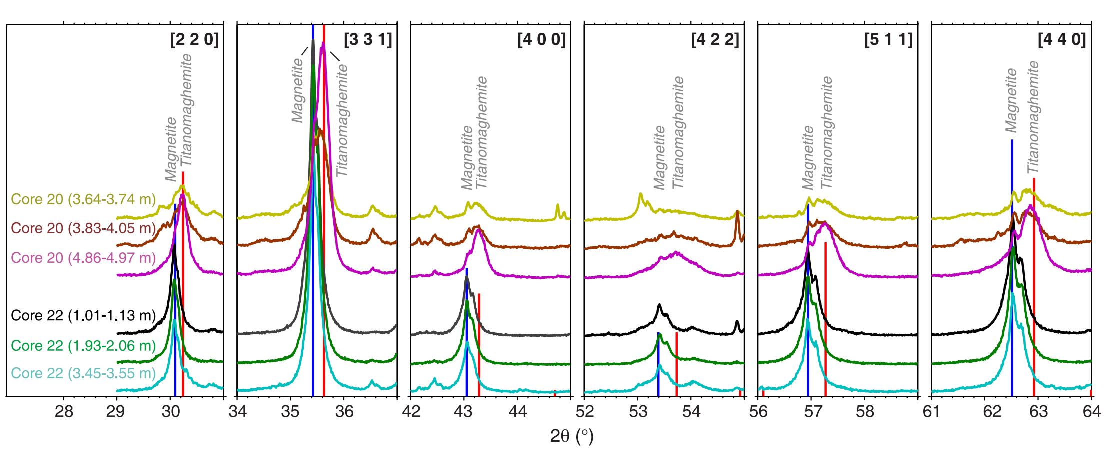

Fig. 13. High resolution XRD results for magnetic extracts from Cores 20 and 22 around the dominant peaks of standard titanomaghemite and magnetite associated with the [2 2 0], [3 1 1], [4 0 0], [4 2 2], [5 1 1], and [4 4 0] hkl diffraction planes. The 2θ positions and magnitudes of XRD peaks for synthetic magnetite and titanomaghemite standards are indicated by vertical blue and red lines, respectively. Note that the minor peak on the high 2θ side of the dominant magnetite peak in Core 22 samples on all diffraction planes is caused by the $K\alpha_{95}$ effect. (For interpretation of the references to colour in this figure legend, the reader is referred to the web version of this article.)

Table 1
2θ values and estimated lattice parameters (L.P.) for (titano)magnetite (tmgt.) and titanomaghemite (tmht.) components derived from the six high-resolution X-ray diffraction peaks in Fig. 13.

Magnetic extracts	Components	Parameters	[h k l] diffraction plane						Mean
			[2 2 0]	[3 1 1]	[4 0 0]	[4 2 2]	[5 1 1]	[4 4 0]	
Core 20	tmgt.	2θ (°)	30.11	35.44	43.08	53.42	56.96	62.55	
3.64–3.74 m		L.P. (Å)	8.3877	8.3936	8.3920	8.3955	8.3936	8.3933	8.3926
	tmht.	2θ (°)	30.25	35.56	43.23	53.71	57.25	62.81	
		L.P. (Å)	8.3498	8.3662	8.3642	8.3536	8.3546	8.3621	8.3584
Core 20	tmgt.	2θ (°)	30.11	35.44	43.1	53.43	56.96	62.56	
3.83–4.05 m		L.P. (Å)	8.3877	8.3936	8.3883	8.3941	8.3936	8.3921	8.3916
	tmht.	2θ (°)	30.24	35.55	43.28	53.68	57.24	62.80	
		L.P. (Å)	8.3525	8.3685	8.3550	8.3579	8.3560	8.3633	8.3589
Core 20	tmgt.	2θ (°)	30.11	35.46	43.08	53.44	56.98	62.56	
4.86–4.97 m		L.P. (Å)	8.3877	8.3890	8.3920	8.3926	8.3909	8.3921	8.3907
	tmht.	2θ (°)	30.25	35.61	43.26	53.72	57.26	62.85	
		L.P. (Å)	8.3498	8.3548	8.3587	8.3521	8.3533	8.3573	8.3543
Core 22	tmgt.	2θ (°)	30.08	35.43	43.05	53.41	56.94	62.53	
1.01–1.13 m		L.P. (Å)	8.3959	8.3959	8.3975	8.3970	8.3963	8.3957	8.3964
Core 22	tmgt.	2θ (°)	30.08	35.42	43.05	53.42	56.94	62.54	
1.93–2.06 m		L.P. (Å)	8.3959	8.3982	8.3975	8.3955	8.3963	8.3945	8.3963
Core 22	tmgt.	2θ (°)	30.07	35.43	43.06	53.41	56.93	62.52	
3.45–3.55 m		L.P. (Å)	8.3986	8.3959	8.3957	8.3970	8.3976	8.3969	8.3969

Mendeleev–Alpha Ridge cores studied by Channell and Xuan (2009), and by Xuan and Channell (2010). For instance, the gradient of IRM acquisition data from Core 20 magnetic extracts show apparent asymmetry, and decomposition of the gradient curves yields two components with mean coercivities close to ~50 mT and ~100 mT, which are very similar to the results of Cores 08 and 10 from the Mendeleev–Alpha Ridge (Xuan and Channell, 2010). The XRD data from Core 20 clearly show two distinct 2θ peaks that correlate well with standard magnetite and titanomaghemite peaks, as has also been observed in Core 08 (Fig. 10 in Xuan and Channell, 2010). Most importantly, thermal demagnetization of the NRM in Core 20 demonstrates that shallow/negative NRM inclination components are carried by titanomaghemite grains that have "unblocking" temperatures largely below 300 °C due to inversion. The x values and oxidation state values (z) of the titanomaghemite in Core 20 meet the requirements (i.e. Readman and O'Reilly, 1972; Nishitani and Kono, 1983) for partial self-reversal in titanomaghemite, as indicated by the EDS (Fig. 12A) and XRD data (Table 1). As for the Mendeleev–Alpha Ridge cores, it is reasonable to interpret the generally shallow NRM inclinations in Core 20, with decimeter thick intervals of low/negative values, to partially self-reversed chemical remanent magnetization (CRM) carried by titanomaghemite formed during seafloor oxidation of host titanomagnetite grains.

For Core 22 from the Yermak Plateau, results from thermal magnetic experiments such as the drop in the medium coercivity component of the three-axis IRM thermal demagnetization data on bulk sediment, the presence of a hump in the susceptibility of magnetic extract samples during heating, and the absence of the hump during cooling, suggest that titanomaghemite grains are also present. The lower amplitude of the medium coercivity component IRM and the smaller hump in susceptibility on heating indicate that Core 22 contains less titanomaghemite than Core 20. The absence of apparent asymmetry in IRM gradient data for Core 22 magnetic extracts is probably due to the following reasons: 1) there is less titanomaghemite in Core 22 sediments, as suggested by the 3-axis IRM thermal demagnetization data; 2) magnetic extraction can be grain-size selective and tend to pull out coarser grains, while finer grains are more likely to have been oxidized to titanomaghemite; 3) only a small proportion (few mg's) of the magnetic extracts was used for the IRM acquisition measurements, and the sample might not be representative. The missing titanomaghemite peaks in XRD are probably also related to the limited sensitivity of the X-ray diffractometer, where concentrations of titanomaghemite may need to exceed a few wt. % to be detected. It is important to point out that thermal demagnetization of the NRM of samples from Core 22 also shows that shallow/negative NRM inclinations are carried by (titanomaghemite) grains that are often largely "unblocked" below 300 °C due to inversion. A partial self-reversed CRM in titanomaghemite grains could also affect NRM inclinations in Core 22, but probably to a lesser extent compared to Core 20 and the Mendeleev–Alpha Ridge cores. This would explain the generally higher quality magnetic data from Core 22 inferred by smaller MAD values, less shift in component NRM inclination from the expected GAD inclination value at the coring site, and more restricted intervals of negative NRM inclinations.

The remarkable similarity of κ_{ARM}/κ from Core 22 to the global benthic oxygen isotope record (Fig. 4A) suggests that κ_{ARM}/κ is a proxy that can be used to constrain the age model in this region, although the mechanism behind this apparent correlation of magnetic grain size to global benthic $\delta^{18}O$ (ice volume signal) needs to be explained. The Yermak Plateau is located on the pathway of the West Spitsbergen Current (WSC) (Fig. 1), which brings Atlantic water into the Arctic Ocean. One possibility is that the observed magnetic grain size variation in Core 22 is modulated by changes in WSC velocity. Although relatively coarse silt grains (10–63 μm) are often used as sortable silt to trace deep-ocean current vigor (e.g., McCave et al., 1995), well-sorted clay to fine silt fractions with peak distribution <10 μm may provide a better proxy for bottom current behavior at locations where significant amounts of silt-sized sediment are supplied by IRD (e.g., Prins et al., 2002). Observations using sediment-trap data collected from the west Svalbard close to Core 22 ('ST' in Fig. 1) indicate that the >10 μm silt fraction is clearly enriched due to IRD released from sea ice (Hebbeln, 2000). The mean sizes of 10–63 μm sortable silt in Core 22 apparently vary with the volume percentages of sortable silt (Fig. 4A) and appear to be inversely related to the population of very fine silt (i.e., 10.64–11.25 μm). This suggests influence of IRD on the 10–63 μm silt at this location. If κ_{ARM}/κ, which is sensitive to fine grains (typically <10 μm), serves as a valid proxy for bottom-current velocity at the Yermak Plateau, the similarity of κ_{ARM}/κ to global benthic $\delta^{18}O$ would indicate coarser magnetic grains and enhanced WSC velocity at lower sea levels during glacial intervals, relative to finer magnetic grains and more sluggish WSC during interglacial high sea levels such as in the Holocene and MIS 5. This pattern implies a sea-level control on current speed in the Fram Strait. One explanation for this control is that lower sea levels and glacial build-up on the Barents Sea shelf could have blocked the Barents Sea branch of Atlantic water inflow, which may have increased the speed of the WSC. Further study on the strength of the two branches of Atlantic water inflow (i.e., WSC and the Barents Sea branch) during glacial and interglacial periods is required to test this potential mechanism. It is also possible that the κ_{ARM}/κ variation in Yermak Plateau cores was driven by changes in sediment sources. For instance, changes in Sr and Nd isotopic composition of sediments from PS 1533 were interpreted to reflect changes in sediment provenance, with more input from the Eurasian shelf during interglacials (through sea-ice transport with the Transpolar Drift) and more input from Svalbard through glacial erosion during times of ice-sheet advance (Tütken et al., 2002). In the central Arctic Ocean, κ_{ARM}/κ may also change with glacial/interglacial variability (O'Regan et al., 2008, 2010), although the details of this co-variation are difficult to discern because of very low sedimentation rates and poorly constrained age models. Nevertheless, this pattern may suggest that κ_{ARM}/κ changes in sediment cores across the Arctic Ocean indicate some fundamental process, possibly related to variability in water exchange between the Arctic and Atlantic oceans.

To check whether NRM inclination data from Core 22 are comparable to other Yermak Plateau cores including Cores PS 1533 and PS 2212 (Nowaczyk et al., 1994), and Core PS 2138 (Nowaczyk and Knies, 2000; Nowaczyk et al., 2003), which recorded several apparent magnetic "excursions", we use κ_{ARM}/κ and radiocarbon ages for correlation. The abrupt increase in κ_{ARM}/κ at a depth of ~4–5.8 m in all four cores provides a stratigraphic marker close to the MIS 5/6 boundary at ~128 kyr. Calibrated radiocarbon ages for three of the cores (except PS 2212 with no ^{14}C ages) introduce another correlation horizon at ~21 kyr (Fig. 6). Mean sedimentation rates estimated based on these stratigraphic tie points are ~3.1–4.5 cm/kyr for the top 4–5.8 m. Considering these sedimentation rates, the Yermak Plateau cores appear anomalously efficient in recording apparent magnetic "excursions", with about 3–4 apparent low/negative NRM inclination intervals recorded in each of these cores during the last ~128 kyr (Fig. 6). Negative inclination intervals in Core PS 2212 appear to occupy almost 50% of the top 4 m of the core. Using the estimated sedimentation rates, the duration of the "Laschamp excursion" in Core PS 2212 reaches >15 kyr, far exceeding the duration estimate of Laj et al. (2000) and the theoretical estimate of excursion duration by Gubbins (1999). Fortuitous variations in sedimentation rates would have to be invoked to explain these low/negative NRM inclinations as magnetic excursions. The unusually high efficiency of the sediments in recording "excursions" and the exceedingly long durations of the recorded "excursions", as well as the lack of a comparable NRM inclination pattern in nearby cores, throw into question the traditional interpretation of shallow/negative NRM inclinations in the Yermak Plateau cores as geomagnetic excursions.

Low-temperature seafloor oxidation is commonly observed in titanomagnetite from deep-sea basalts (e.g., Ozima and Larson, 1970; Zhou et al., 2001), and self-reversed NRM components carried by the oxidized titanomaghemite have been reported (i.e. Doubrovine and Tarduno, 2004). Oxidation of magnetite to maghemite is common in the oxic surface sediment layer in deep-sea sediments (e.g., Smirnov and Tarduno, 2000), but oxidized rims usually undergo dissolution as the sediment gets buried below the surface oxic zone. Oxidizing diagenetic conditions exist at much greater depth in these Arctic deep-sea sediments, as reflected in the predominance of dark-brown (manganese-hydroxide enriched), organic-poor, sediments. These conditions are consistent with the combination of low sediment accumulation rates (mostly less than 1 cm/kyr, see Polyak et al., 2009; Stein et al., 2010) and low fluxes of labile organic matter under perennial ice cover. On the Yermak Plateau, diagenetic oxidation is less prevalent than in the central Arctic Ocean, as indicated by larger lattice parameters of the titanomagnetite component (see Table 1). Less oxidizing conditions on the Yermak Plateau are consistent with higher fluxes of labile organic matter and higher sedimentation rates due to more seasonal rather than perennial ice cover in this area (see Fig. 1).

The observed NRM inclinations in Arctic deep-sea sediments may depend on several factors including the degree of diagenetic oxidation of individual grains that carry the primary detrital remanent magnetization (DRM) and the over-printing of a diagenetic CRM on the original DRM. The oxidation of grains that carry the original DRM is controlled by the redox conditions in the sediments, which are, in turn, controlled by the activity of (sulfate) reducing microbes. The low activity of sulfate reducers in Arctic Ocean sediments is probably due to low concentrations of labile organic matter at least down to ~200 mbsf, with a possible contribution from dissolution of gypsum at larger sediment depths (Backman et al., 2005). Variations in sedimentation rates, as well as changes in magnetic grain size (finer grains have greater surface area to volume ratio) may also affect the degree of downcore alteration of the magnetic records. Lower deposition rates and finer magnetic grains may lead to higher degree of oxidation, therefore more distortion of NRM in the sediments.

Changes in the strength of the ambient magnetic field add further variability to the resulting NRM inclination through the alignment efficiency of grains that contribute to the DRM. For instance, according to the tentative age model of Core 22 based on correlating κ_{ARM}/κ data to the PISO-1500 oxygen isotope stack, the shallow and negative inclination intervals in Core 22 appear to occur in the vicinity of paleointensity minima in the paleointensity reference curve associated with the PISO-1500 stack (Fig. 7). Although this observation needs to be constrained by more definitive chronology, a possible explanation is that strength of the geomagnetic field modulates the alignment efficiency of magnetic grains in sediments. During the times of weak geomagnetic field, only finer magnetic grains were aligned with the ambient field. As finer grains are more likely to undergo maghemitization due to their larger surface area to volume ratio, they contribute preferentially to the CRM that distorts the NRM record.

Acknowledgments

We thank Kainian Huang for help with magnetic measurements, Ann Heatherington for SEM assistance, Gianna Browne and Jason Curtis for help with oxygen isotope analyses, and Matt O'Regan for providing the κ_{ARM}/κ data of ACEX. We also thank two anonymous reviewers for constructive comments. This research project was supported by the US National Science Foundation through awards ARC-0806309, ARC-0806999, and ARC-0806857.

References

Backman, J., Jakobsson, M., Løvlie, R., Polyak, L., Febo, L.A., 2004. Is the central Arctic Ocean a sediment starved basin? Quat. Sci. Rev. 23, 1435–1454.

Backman, J., Moran, K., McInroy, D., IODP Expedition 302 Scientists, 2005. IODP expedition 302, Arctic coring expedition (ACEX): a first look at the Cenozoic paleoceanography of the central Arctic Ocean. Sci. Drill. 1, 12–17. doi:10.2204/iodp.sd.1.02.2005.

Backman, J., Jakobsson, M., Frank, M., Sangiorgi, F., Brinkhuis, H., Stickley, C., O'Regan, M., Løvlie, R., Pälike, H., Spofforth, D., Gattacecca, J., Moran, K., King, J., Heil, C., 2008. Age model and core-seismic integration for the Cenozoic Arctic coring expedition sediments from the Lomonosov ridge. Palaeoceanography 23, PA1S03. doi:10.1029/ 2007PA001476.

Björk, G., Jakobsson, M., Rudels, B., Swift, J.H., Anderson, L., Darby, D.A., Backman, J., Coakley, B., Winsor, P., Polyak, L., Edwards, M., 2007. Bathymetry and deep-

water exchange across the central Lomonosov Ridge at 88°–89°N. Deep-Sea Res. 54, 1197–1208.
Bleil, U., Gard, G., 1989. Chronology and correlation of Quaternary magnetostratigraphy and nannofossil biostratigraphy in Norwegian–Greenland Sea sediments. Geol. Rundschau 78, 1173–1187.
Champion, D.E., Lanphere, M.A., Kuntz, M.A., 1988. Evidence for a new geomagnetic reversal from lava flows in Idaho: discussion of short polarity reversals in the Brunhes and late Matuyama Chrons. J. Geophys. Res. 93, 11667–11680.
Channell, J.E.T., Xuan, C., 2009. Self-reversal and apparent magnetic excursions in Arctic sediments. Earth Planet. Sci. Lett. 284, 124–131.
Channell, J.E.T., Xuan, C., Hodell, D.A., 2009. Stacking paleointensity and oxygen isotope data for the last 1.5 Myrs (PISO-1500). Earth Planet. Sci. Lett. 283, 14–23.
Clark, D.L., 1970. Magnetic reversals and sedimentation rates in the Arctic Basin. Geol. Soc. Amer. Bull. 81, 3129–3134.
Darby, D.A., Bischof, J.F., Jones, G.A., 1997. Radiocarbon dating of depositional regimes in the western Arctic Ocean. Deep-Sea Res. 44, 1745–1757.
Darby, D.A., Ortiz, J., Polyak, L., Lund, S., Jakobsson, M., Woodgate, R.A., 2009. The role of currents and sea ice in both slowly deposited central Arctic and rapidly deposited Chukchi-Alaskan margin sediments. Glob. Planet. Change 68, 58–72.
Day, R., Fuller, M., Schmidt, V.A., 1977. Hysteresis properties of titanomagnetites: grainsize and compositional dependence. Phys. Earth Planet. Int. 13, 260–267.
Doubrovine, P.V., Tarduno, J.A., 2004. Self-reversed magnetization carried by titanomaghemite in oceanic basalts. Earth Planet. Sci. Lett. 222, 959–969.
Doubrovine, P.V., Tarduno, J.A., 2006. Alteration and self-reversal in oceanic basalts. J. Geophys. Res. 111, B12S30. doi:10.1029/2006JB004468.
Frank, M., Backman, J., Jakobsson, M., Moran, K., O'Regan, M., King, J., Haley, B.A., Kubik, P.W., Garbe-Schönberg, D., 2008. Beryllium isotopes in central Arctic Ocean sediments over the past 12.3 million years: stratigraphic and paleoceanographic implications. Paleoceanography 23, PA1S02. doi:10.1029/2007PA001478.
Gravenor, C.P., Symons, D.T.A., Coyle, D.A., 1984. Errors in the anisotropy of magnetic susceptibility and magnetic remanence of unconsolidated sediments produced by sampling methods. Geophys. Res. Lett. 11, 836–839.
Gubbins, D., 1999. The distinction between geomagnetic excursions and reversals. Geophys. J. Int. 137, F1–F3.
Hamilton, N., Rees, A.I., 1970. The use of magnetic fabric on the interpretation of polarity records in deep-sea in palaeocurent estimation. In: Runcorn, S.K. (Ed.), Sediments. Palaeogeophysics. Academic Press, London, p. 518.
Harrison, R.J., Feinberg, J.M., 2008. FORCinel: an improved algorithm for calculating first-order reversal curve distributions using locally weighted regression smoothing. Geochem. Geophys. Geosyst. 9, Q05016. doi:10.1029/2008GC001987.
Hebbeln, D., 2000. Flux of ice-rafted detritus from sea-ice in the Fram Strait. Deep-Sea Res. 47, 1773–1790.
Herman, Y., 1974. Arctic Ocean sediments, microfauna, and the climatic record in late Cenozoic time. In: Herman, Y. (Ed.), Marine Geology and Oceanography of the Arctic Seas. Springer-Verlag, Berlin, pp. 283–348.
Heslop, D., Dekkers, M.J., Kruiver, P.P., van Oorschot,, I.H.M., 2002. Analysis of isothermal remanent magnetization acquisition curves using the expectation-maximization algorithm. Geophys. J. Int. 148, 58–64.
Hunkins, K.L., Bé, A.W.H., Opdyke, N.D., Mathieu, G., 1971. The late Cenozoic history of the Arctic Ocean. In: Turekian, K.K. (Ed.), The Late Cenozoic Glacial Ages. Yale Univ. Press, pp. 215–237.
Jakobsson, M., Løvlie, R., Al-Hanbali, H., Arnold, E., Backman, J., Mörth, M., 2000. Manganese and color cycles in Arctic Ocean sediments constrain Pleistocene chronology. Geology 28, 23–26.
Jakobsson, M., Løvlie, R., Arnold, E.M., Backman, J., Polyak, L., Knutsen, J.O., Musatov, E., 2001. Pleistocene stratigraphy and paleoenvironmental variation from Lomonsov Ridge ediments, central Arctic Ocean. Glob. Planet. Change 31, 1–22.
Jakobsson, M., Backman, J., Murray, A., Løvlie, R., 2003. Optically Stimulated Luminescence dating supports central Arctic Ocean cm-scale sedimentation rates. Geochem. Geophys. Geosyst. 4, 1016. doi:10.1029/2002GC000423.
Jakobsson, M., Macnab, R., Mayer, M., Anderson, R., Edwards, M., Hatzky, J., Schenke, H.W., Johnson, P., 2008. An improved bathymetric portrayal of the Arctic Ocean: implications for ocean modeling and geological, geophysical and oceanographic analyses. Geophys. Res. Lett. 35, L07602. doi:10.1029/2008GL033520.
Jelínek, V., Kropáček, V., 1978. Statistical processing of anisotropy of magnetic susceptibility measured on groups of specimens. Stud. Geophys. Geod. 22, 50–62.
Kaufman, D.S., Polyak, L., Adler, R., Channell, J.E.T., Xuan, C., 2008. Dating late Quaternary planktonic foraminifer *Neogloboquadrina pachyderma* from the Arctic Ocean by using amino acid racemization. Paleoceanography 23, PA3224. doi:10.1029/2008PA001618.
King, J.W., Banerjee, S.K., Marvin, J., 1983. A new rock-magnetic approach to selecting sediments for geomagnetic paleointensity studies: application to paleointensity for the last 4000 years. J. Geophys. Res. 88, 5911–5921.
Kirschvink, J.L., 1980. The least squares lines and plane analysis of paleomagnetic data. Geophys. J. R. Astr. Soc. 62, 699–718.
Knies, J., Vogt, C., Stein, R., 1999. Late Quaternary growth and decay of the Svalbard–Barents Sea ice sheet and paleoceanographic evolution in the adjacent Arctic Ocean. Geo-Mar. Lett. 18, 195–202.
Laj, C., Channell, J.E.T., 2007. Geomagnetic excursions. In: Kono, M. (Ed.), 2007. Treatise on Geophysics. Geomagnetism, vol. 5. Elsevier, Amsterdam, pp. 373–416.
Laj, C., Kissel, C., Mazaud, A., Channell, J.E.T., Beer, J., 2000. North Atlantic paleointensity stack since 75 ka (NAPIS-75) and the duration of the Laschamp event. Phil. Trans. R. Soc. Lond. A 358, 1009–1025.
Langereis, C.G., Dekkers, M.J., de Lange, G.J., Paterne, M., van Santvoort, P.J.M., 1997. Magnetostratigraphy and astronomical calibration of the last 1.1 Myr from an eastern Mediterranean piston core and dating of short events in the Brunhes. Geophys. J. Int. 129, 75–94.
Løvlie, R., Markussen, B., Sejrup, H.P., Thiede, J., 1986. Magnetostratigraphy in three Arctic Ocean sediment cores; arguments for magnetic excursions within oxygen isotope stage 2–3. Phys. Earth Planet. Inter. 43, 173–184.
Lowrie, W., 1990. Identification of ferromagnetic minerals in a rock by coercivity and unblocking temperature properties. Geophys. Res. Lett. 17, 159–162.
Lund, S.P., Acton, G.D., Clement, B.M., Okada, M., Williams, T., 2001. Paleomagnetic records of Stage 3 excursions. Leg 172. In: Keigwin,, L.D., Rio,, D., Acton,, G.D., Arnold,, E. (Eds.), Proc. ODP Sci. Results, 172. Ocean Drilling Program, College Station, TX, pp. 1–20.
Lund, S., Stoner, J.S., Channell, J.E.T., Acton, G., 2006. A summary of Brunhes paleomagnetic field variability recorded in Ocean Drilling Program cores. Phys. Earth Planet. Inter. 156, 194–204.
McCave, I.N., Manighetti, B., Robinson, S.G., 1995. Sortable silt and fine sediment size/composition slicing: parameters for paleocurrent speed and paleoceanography. Paleoceanography 10, 593–610.
McCave, I.N., Hall, I.R., Bianchi, G.G., 2006. Laser vs settling velocity differences in silt grainsize measurements: estimation of palaeocurrent vigour. Sedimentology 53, 919–928.
Nishitani, T., Kono, M., 1983. Curie temperature and lattice constant of oxidized titanomagnetite. Geophys. J. R. Astron. Soc. 74, 585–600.
Nowaczyk, N.R., Antonow, M., 1997. High resolution magnetostratigraphy of four sediment cores from the Greenland Sea – I. Identification of the Mono Lake excursion, Laschamp and Biwa I/Jamaica geomagnetic polarity events. Geophys. J. Int. 131, 310–324.
Nowaczyk, N.R., Baumann, M., 1992. Combined high-resolution magnetostratigraphy and nannofossil biostratigraphy for late Quaternary Artic Ocean sediments. Deep Sea Res. 39, 567–601.
Nowaczyk, N.R., Frederichs, T.W., 1999. Geomagnetic events and relative paleointensity variations during the last 300 ka as recorded in Kolbeinsey Ridge Sediments, Iceland Basin – indication for a strongly variable geomagnetic field. Int. J. Earth Sci. 88, 116–131.
Nowaczyk, N.R., Knies, J., 2000. Magnetostratigraphic results from the eastern Arctic Ocean: aMS ^{14}C ages and relative paleointensity data of the Mono Lake and Laschamp geomagnetic reversal excursions. Geophys. J. Int. 140, 185–197.
Nowaczyk, N.R., Frederichs, T.W., Eisenhauer, A., Gard, G., 1994. Magnetostratigraphic data from late Quaternary sediments from the Yermak Plateau, Arctic Ocean: evidence for four geomagnetic polarity events within the last 170 Ka of the Brunhes Chron. Geophys. J. Int. 117, 453–471.
Nowaczyk, N.R., Frederichs, T.W., Kassens, H., Nørgaard-Pedersen, N., Spielhagen, R.F., Stein, R., Weiel, D., 2001. Sedimentation rates in the Makarov basin, central Arctic Ocean: a paleomagnetic and rock magnetic approach. Paleoceanography 16, 368–389.
Nowaczyk, N.R., Antonow, M., Knies, J., Spielhagen, R.F., 2003. Further rock magnetic and chronostratigraphic results on reversal excursions during the last 50 ka as derived from northern high latitudes and discrepancies in precise AMS ^{14}C dating. Geophys. J. Int. 155, 1065–1080.
O'Regan, M., King, J., Backman, J., Jakobsson, M., Palike, H., Moran, K., Heil, C., Sakamoto, T., Cronin, T.M., Jordan, R.W., 2008. Constraints on the Pleistocene chronology of sediments from the Lomonosov Ridge. Paleoceanography 23, PA1S19. doi:10.1029/2007PA001551.
O'Regan, M., St. John, K., Moran, K., Backman, K., King, J., Haley, B.A., Jakobsson, M., Frank, M., Röhl, U., 2010. Plio-Pleistocene trends in ice-rafted debris on the Lomono-sov Ridge. Quaternary Int. 219, 168–176.
Ozima, M., Larson, E.E., 1970. Low- and high-temperature oxidation of titanomagnetite in relation to irreversible changes in the magnetic properties of submarine basalts. J. Geophys. Res. 75, 1003–1017.
Polyak, L., Bischof, J., Ortiz, J.D., Darby, D.A., Channell, J.E.T., Xuan, C., Kaufman, D.S., Løvlie, R., Schneider, D.A., Eberl, D.D., Adler, R.E., Council, E.A., 2009. Late Quaternary stratigraphy and sedimentation patterns in the western Arctic Ocean. Glob. Planet. Change 68, 5–17.
Prins, M.A., Bouwer, L.M., Beets, C.J., Troelstra, S.R., Weltje, G.J., Kruk, R.W., Kuijpers, A., Vroon, P.Z., 2002. Ocean circulation and iceberg discharge in the glacial North Atlantic: inferences from unmixing of sediment size distributions. Geology 30, 555–558.
Readman, P.W., O'Reilly, W., 1972. Magnetic properties of oxidized (cation deficient) titanomagnetites $(Fe, Ti, \square)_3 O_4$. J. Geomagn. Geoelectr. 24, 69–90.
Roberts, A.P., Winklhofer, M., 2004. Why are geomagnetic excursions not always recorded in sediments? Constraints from post-depositional remanent magnetization lock-in modelling. Earth Planet. Sci. Lett. 227, 345–359.
Rochette, P., Jackson, M., Aubourg, C., 1992. Rock magnetism and the interpretation of anisotropy of magnetic susceptibility. Rev. Geophys. 30, 209–226. doi:10.1029/92RG00733.
Sellén, E., O'Regan, M., Jakobsson, M., 2010. Spatial and temporal Arctic Ocean depositional regimes: a key to the evolution of ice drift and current patterns. Quat. Sci. Rev. 29, 3644–3664.
Smirnov, A.V., Tarduno, J.A., 2000. Low-temperature magnetic properties of pelagic sediments (Ocean Drilling Program Site 805C): tracers of maghemitization and magnetic mineral reduction. J. Geophys. Res. 105, 16457–16471.

Spielhagen, R.F., Baumann, K.H., Erlenkeuser, H., Nowaczyk, N.R., Nørgaard-Pedersen, N., Vogt, C., Weiel, D., 2004. Arctic Ocean deep-sea record of northern Eurasian ice sheet history. Quat. Sci. Rev. 23, 1455–1483.
Stein, R., Matthiessen, J., Niessen, F., Krylov, A., Nam, S., Bazhenova, E., 2010. Towards a better (litho-) stratigraphy and reconstruction of Quaternary paleoenvironment in the Amerasian Basin (Arctic Ocean). Polarforschung 79, 97–121.
Steuerwald, B.A., Clark, D.L., Andrew, J.A., 1968. Magnetic stratigraphy and faunal patterns in Arctic Ocean sediments. Earth Planet. Sci. Lett. 5, 79–85.
Thomas, R., Guyodo, Y., Channell, J.E.T., 2003. U-channel track for susceptibility measurements. Geochemistry. Geophys. Geosys. 4, 1050. doi:10.1029/2002GC000454.
Tütken, T., Eisenhauer, A., Wiegand, B., Hansen, B., 2002. Glacial–interglacial cycles in Sr and Nd isotopic composition of Arctic marine sediments triggered by the Svalbard/Barents Sea ice sheet. Mar. Geol. 182, 351–372.
Wang, R., Løvlie, R., 2008. SP-grain production during thermal demagnetization of some Chinese loess/palaeosol. Geophys. J. Int. 172, 504–512.
Witte, W.K., Kent, D.V., 1988. Revised magnetostratigraphies confirm low sedimentation rates in Arctic Ocean cores. Quat. Res. 29, 43–53.
Worm, H.U., 1997. A link between geomagnetic reversals and events and glaciations. Earth Planet. Sci. Lett. 147, 55–67.
Xuan, C., Channell, J.E.T., 2009. UPmag: MATLAB software for viewing and processing u-channel or other pass-through paleomagnetic data. Geochem. Geophy. Geosyst. 10, Q10Y07. doi:10.1029/2009GC002584.
Xuan, C., Channell, J.E.T., 2010. Origin of apparent magnetic excursions in deep-sea sediments from Mendeleev–Alpha Ridge (Arctic Ocean). Geochem. Geophy. Geosyst. 11, Q02003. doi:10.1029/2009GC002879.
Zhou, W., Van der Voo, R., Peacor, D.R., Wang, D., Zhang, Y., 2001. Low temperature oxidation in MORB of titanomagnetite to titanomaghemite: a gradual process with implications for marine magnetic anomaly amplitudes. J. Geophys. Res. 106, 6409–6421.